Journal of Medicinal Chemistry

Article

pubs.acs.org/jmc

Design and Synthesis of a Pan-Janus Kinase Inhibitor Clinical Candidate (PF-06263276) Suitable for Inhaled and Topical Delivery for the Treatment of Inflammatory Diseases of the Lungs and Skin

Peter Jones,[*,†,#] R. Ian Storer,[*,#,◆] Yogesh A. Sabnis,[#,¶] Florian M. Wakenhut,[#,∞] Gavin A. Whitlock,[#,×] Katherine S. England,[#,◇] Takasuke Mukaiyama,[#,△] Christoph M. Dehnhardt,[†,▲] Jotham W. Coe,[∥] Steve W. Kortum,[∥] Jill E. Chrencik,[∥] David G. Brown,[▽,∀] Rhys M. Jones,[‡] John R. Murphy,[○] Thean Yeoh,[⊥] Paul Morgan,[§] and Iain Kilty[§]

[†]Medicine Design, [‡]Pharmacokinetics, Dynamics and Metabolism, and [§]Inflammation and Immunology Research Unit, Pfizer Inc., 610 Main Street, Cambridge, Massachusetts 02139, United States

[∥]Medicine Design, and [⊥]Medicinal Sciences, Pfizer Inc., 445 Eastern Point Road, Groton, Connecticut 06340, United States

[#]Worldwide Medicinal Chemistry, [▽]Structural Biology and Biophysics, and [○]Pharmaceutical Sciences, Pfizer Ltd., Ramsgate Road, Sandwich, CT13 9NJ, U.K.

Supporting Information

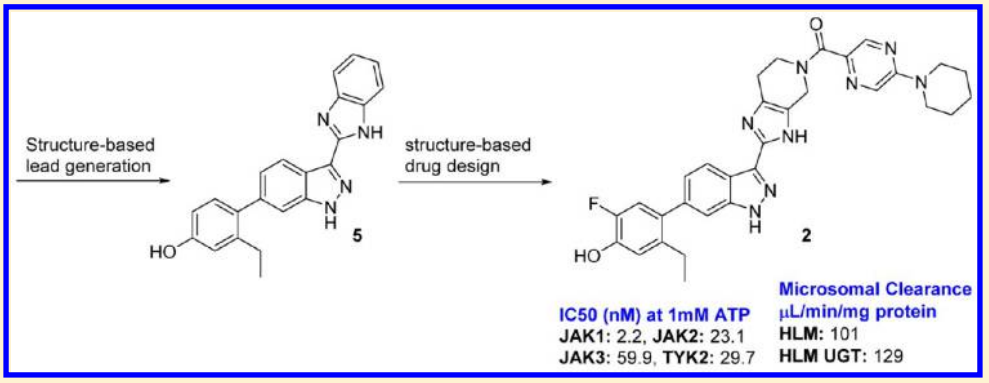

ABSTRACT: By use of a structure-based computational method for identification of structurally novel Janus kinase (JAK) inhibitors predicted to bind beyond the ATP binding site, a potent series of indazoles was identified as selective pan-JAK inhibitors with a type 1.5 binding mode. Optimization of the series for potency and increased duration of action commensurate with inhaled or topical delivery resulted in potent pan-JAK inhibitor **2** (PF-06263276), which was advanced into clinical studies.

INTRODUCTION

Janus kinases, JAKs, are a family of tyrosine kinases comprising four members (JAK1, -2, -3, and Tyk2). They play a critical role in both innate and adaptive immunity, since they function as key transducers in the signaling processes of many cytokine receptors.[1] As such, they have emerged as attractive targets for a number of inflammatory diseases, and numerous inhibitors are under active clinical development.[2] Among these, tofacitinib, **1** (Figure 1) was first approved in 2012 by the FDA for the treatment of rheumatoid arthritis (RA).[3] The efficacy and safety of tofacitinib has been studied in several immune-mediated inflammatory diseases, including rheumatoid arthritis,[4] psoriasis,[5] ulcerative colitis,[6] Crohn's disease,[7] psoriatic arthritis,[8] and ankylosing spondylitis.[9]

By use of JAK enzymatic assays run at physiologically relevant 1 mM ATP concentration, tofacitinib displays selectivity for JAK1 inhibition, although it also inhibits JAK3 (3-fold weaker) and JAK2 (5-fold weaker). In a cellular settting, tofacitinib preferentially inhibits signaling by heterodimeric cytokine receptors that associate with JAK3 and/or JAK1 with functional selectivity over cytokine receptors that signal via

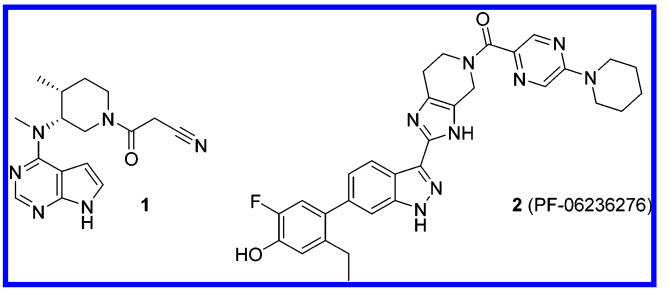

Figure 1. Structures of tofacitinib (**1**) and novel pan-JAK inhibitor (**2**).

Received: November 8, 2016
Published: December 16, 2016

DOI: 10.1021/acs.jmedchem.6b01634
J. Med. Chem. XXXX, XXX, XXX−XXX

Table 1. Potency and in Vitro Metabolic Stability Data for Tofacitinib Analogues 3 and 4

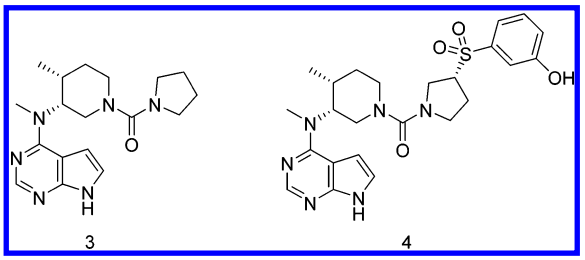

	IC_{50}[a] (nM)					
compd	JAK1	JAK2	JAK3	Tyk2	HLM[b] ((μL/min)/mg protein)	HLM UGT[c] ((μL/min)/mg protein)
3	37.5	123.6	139.3	1632.2	82	<3.5
4	2.3	21.2	34.1	958.6	131	>200

[a]Compounds were routinely assayed using Caliper microfluidic assays for their potency of inhibition of phosphorylation of a peptide substrate by the appropriate JAK enzyme at 1 mM ATP concentration. All IC_{50} values reported represent geometric mean values of a minimum of three determinations. [b]Compounds were routinely assessed for metabolic stability in human liver microsomes (HLMs). [c]Compounds were assessed for phase II glucuronidation in HLM by including the microsomal activator Brij58 and cofactor uridine diphosphate glucuronic acid (UDPGA) and excluding the cytochrome P450 dependent cofactor NADPH.

pairs of JAK2. For example in human whole blood assays, tofacitinib inhibits IL-15, IFNα, and IL-6 signaling with IC_{50} values between 35 and 80 nM, whereas the IC_{50} for JAK2 dependent EPO signaling was ∼300 nM. Given the role of JAK2 dependent EPO signaling in red blood cell production, reduction in hemoglobin levels was observed at higher doses with tofacitinib in clinical trials.[2] Despite this, the functional selectivity for cytokine inhibition for EPO signaling has proven to be manageable at clinical doses that provide benefit to rheumatoid arthritis and psoriasis patients without reducing hemoglobin.[4a,10]

There are a number of JAK inhibitors in clinical development that have varying selectivities within the JAK family. In a cellular setting the advanced candidates preferentially inhibit JAK1 dependent cytokines, including the γ-common chain cytokines, interferons, and IL-6.[2] Since tofacitinib and other JAK inhibitor advanced clinical candidates preferentially inhibit JAK1-dependent cytokines, little clinical differentiation is expected. To further improve upon the therapeutic potential of JAK inhibition in general, a greater degree of selectivity over systemic JAK2 inhibition and EPO signaling in particular would be desirable. Besides attempting to produce an inhibitor with higher selectivity among the JAK family, an alternative approach for certain diseases would be to target JAK inhibition directly at the site of action in the relevant organ of interest while avoiding widespread systemic JAK inhibition. Herein we describe the design and development of a novel and potent pan-JAK inhibitor **2** (PF-06263276, Figure 1),[11] suitable for inhaled or topical administration as an organ targeted therapy. Compound **2** has the potential to treat inflammatory diseases of the lungs (such as COPD)[12] and skin (such as mild-to-moderate psoriasis)[5a] with negligible systemic JAK inhibition.

RESULTS AND DISCUSSION

Following our previously described concept of "inhalation by design",[13] we sought to design a JAK inhibitor that fulfilled the following criteria: (1) high potency to minimize dose size, given the limits of dose sizes of typical dry powder inhalation (DPI) devices (<1 mg drug product) and to minimize the percentage of active ingredient required in topical formulations, (2) high selectivity for the JAK family of kinases versus the rest of the kinome, (3) low systemic exposure and high metabolic clearance to maximize the therapeutic index by targeting drug only to the site of action (with no potent active metabolites formed), (4) multiple routes and mechanisms of metabolism to minimize the potential for any drug−drug interactions, (5) suitable solid form characteristics to allow for blending with lactose for use in a DPI device and formulation as a topical ointment or cream, (6) evidence of long duration of action (DoA) of JAK inhibition in enzymatic assays (through kinetic experiments) or cell based assays (through cell wash-out experiments), to allow for sustained target modulation in vivo.

Given the successful clinical precedent of tofacitinib to modulate JAK driven disease, our initial tactic was to increase the lipophilicity in this template to introduce metabolic instability, with the aim to maintain or improve the significant JAK potency and selectivity typically observed with this chemotype, while also assaying for evidence of DoA. We quickly found that a urea linkage could be used in place of the amide bond in tofacitinib, and this allowed for facile introduction of lipophilic groups that maintained excellent JAK potency and selectivity while introducing metabolic instability. For example **3** (PF-00956980), a useful commercially available JAK inhibitor tool, (Table 1) maintains excellent JAK potency and has high turnover in human liver microsomes (HLM).[14] The pyrrolidine ring of **3** could be further substituted with no loss in potency by larger groups containing phenols, which were introduced to allow for rapid phase II metabolism of compounds, thus providing a second route of metabolism. For example **4** (Table 1) has high turnover in both HLM and HLM UGT assays and increased JAK enzyme potency relative to compound **3**.

Urea **4** was shown to have a suitable crystalline solid form and acceptable thermodynamic solubility (20 μg/mL) to meet our initial compound criteria; however in a number of different assay formats we could not demonstrate evidence for significant DoA with this compound nor with any others within this chemotype. To investigate enzyme inhibition kinetics, we used a continuous JAK3 dilution recovery assay using microfluidic mobility shift assay technology.[15] Both tofacitinib **1** and urea **3** showed no evidence of slow-offset from JAK3 in this assay, while **4** showed an offset rate of 0.024 min^{-1} that translated to a $T_{1/2}$ of approximately 28 min. In a PBMC cell-based assay we could measure inhibition of the cellular pSTAT5 response to

DOI: 10.1021/acs.jmedchem.6b01634
J. Med. Chem. XXXX, XXX, XXX−XXX

IL-2 stimulation with **3** and **4** giving IC_{50} values of 27 nM and 343 nM, respectively. Using this assay, we investigated cellular DoA by incubating compounds for 1 h at 10-fold the IC_{50}, washing cells extensively, and then monitoring recovery of the cellular pSTAT5 response to IL-2 stimulation over time. Both **3** and **4** showed no sign of pSTAT5 inhibition in this assay immediately following cell washing. Assessing these data together, we did not view these compounds as having significant potential to show clinical duration of action as inhaled or topical agents in vivo, and thus we sought an alternative chemical series.

Examination of overlaid X-ray crystal structures of tofacitinib **1** and **4** bound to JAK2 (Figure 2) shows that they both adopt

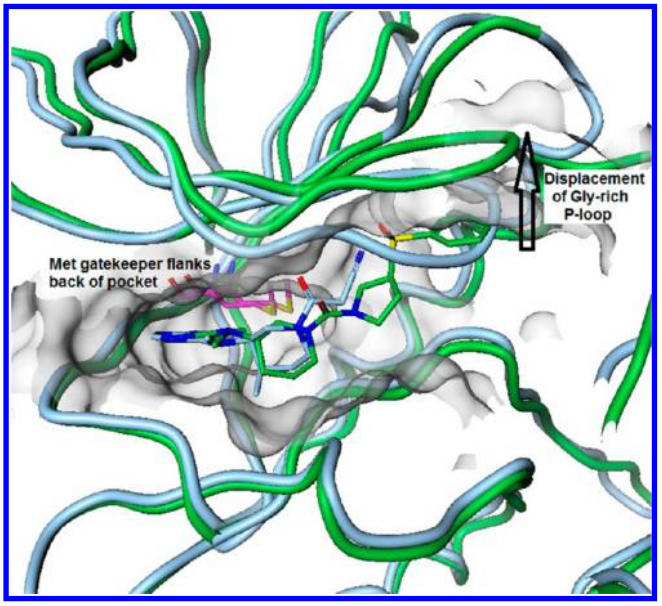

Figure 2. Overlaid X-ray cocrystal structures illustrating binding mode of tofacitinib (**1**) (PDB entry 3LXK) and **4** (PDB entry 5TQ7) bound to JAK2.

the same "type-1" inhibitor binding mode with the methionine gatekeeper residue flanking the back of the pocket in both cases.[16] The larger molecule **4** shows some displacement of the glycine rich P-loop of the kinase relative to tofacitinib, although as demonstrated by our data, this binding mode does not appear to result in any significant kinetic advantage, likely due to high flexibility of the protein in this region.

It has been well documented by us and others that certain kinase inhibitor binding modes appear to be correlated to slow-offset binding kinetics, in particular the "type 2" inhibitor binding mode.[13c,16] This binding mode results in a portion of the inhibitor binding at a remote distance from the hinge binding motif, behind the gatekeeper amino acid, into an induced "back pocket" of the kinase, resulting in significant movement of the DFG portion of the activation loop and stabilization of an inactive form of the kinase. In order to find a JAK inhibitor series with evidence of DoA in enzyme kinetics and cell based experiments, we sought to leverage our internal database of kinase X-ray cocrystal structures, along with kinase cocrystal structures available from the PDB,[17] to identify a subset of kinase inhibitors with the potential to bind behind the gatekeeper residue and to screen this subset for potency against the JAK kinases.

Using approximately 2500 in-house kinase inhibitor crystal structures, together with approximately 1500 additional structures available from the PDB, we computationally collected and aligned all structures into a common orientation. A computational triage was then performed to identify any inhibitor templates that were predicted to bind to the hinge region of the kinase and within 2 Å of the methionine gatekeeper residue in JAK3. We reasoned that any compounds found to be potent JAK inhibitors from this selection would likely bind in a manner necessitating a conformational change in the kinase, placing binding elements in the back pocket of the kinase, potentially leading to slower offset kinetics. This screening effort resulted in the discovery that the indazole-phenol **5** (Table 2), a compound in our corporate collection from a previous research program,[18] is a potent pan-JAK inhibitor with IC_{50} values of <1 nM to 10 nM against the JAK kinase family at 1 mM ATP concentration. **5** displayed an enzymatic kinetic offset rate of 0.006 min^{-1} that translated to a $T_{1/2}$ of approximately 114 min for JAK3. It also showed a significant time dependent inhibition of the cellular pSTAT5 response to IL-2 stimulation following compound incubation and cell washing, with a $T_{1/2}$ of 6.5 h.

We were pleased to find that an X-ray crystal structure of **5** bound to JAK2 (Figure 3) showed a novel binding mode for

Table 2. Profile of Indazole-phenol 5

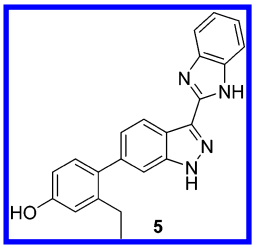

5

	IC_{50} [a] (nM)					
compd	JAK1	JAK2	JAK3	Tyk2	HLM[b] ((μL/min)/mg protein)	HLM UGT[c] ((μL/min)/mg protein)
5	0.4	2.2	8.3	9.1	35	49

[a]Compounds were routinely assayed using Caliper microfluidic assays for their potency of inhibition of phosphorylation of a peptide substrate by the appropriate JAK enzyme at 1 mM ATP concentration. All IC_{50} values reported represent geometric mean values of a minimum of three determinations. [b]Compounds were routinely assessed for metabolic stability in human liver microsomes (HLMs). [c]Compounds were assessed for phase II glucuronidation in HLM by including the microsomal activator Brij58 and cofactor uridine diphosphate glucuronic acid (UDPGA) and excluding the cytochrome P450 dependent cofactor NADPH.

DOI: 10.1021/acs.jmedchem.6b01634
J. Med. Chem. XXXX, XXX, XXX−XXX

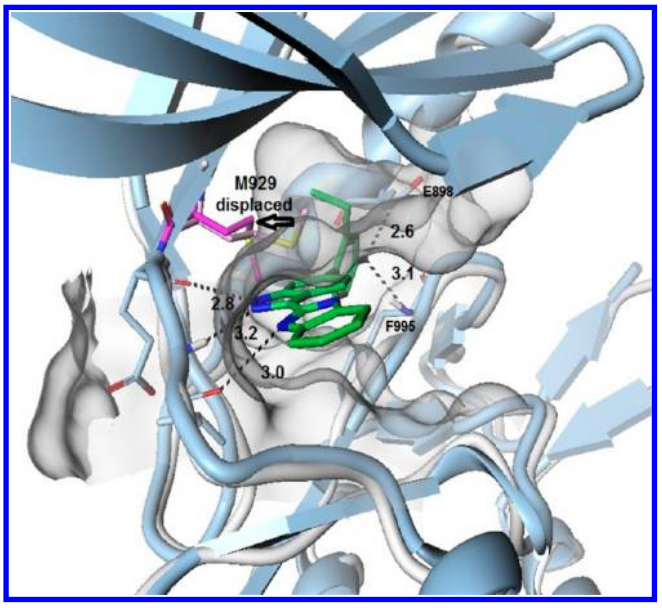

Figure 3. X-ray cocrystal structure of **5** bound to JAK2 (PDB entry 5TQ3) overlaid on protein from cocrystal with **4** to illustrate movement of the methionine gatekeeper residue. Numbers correspond to hydrogen bonding distances in angstroms.

the JAK kinases, compared to the previously observed type-1 binding mode observed with tofacitinib. The methionine gatekeeper residue moved approximately 4.3 Å from the known type-1 binding mode orientation, allowing the phenolic portion of the molecule to bind behind the gatekeeper in an induced back pocket. The indazole-benzimidazole portion of the molecule forms three hydrogen bonding interactions with the hinge region of the kinase, while the phenol group makes two hydrogen bonding interactions in the back-pocket, with the α-Glu (E898) of the C-helix and the backbone NH of the Phe (F995) of the DFG motif. The ethyl group of the phenol ring occupies the lipophilic space left by movement of the methionine side chain and helps induce a twist across the biaryl bond to the indazole ring. It is interesting to note that despite significant binding in the backpocket and the movement of the gatekeeper methionine, the DFG motif has not moved significantly and that this structure does not represent a type-2 binding mode. Similar binding modes have been described previously for other kinases as type 1.5.[19] On the basis of this binding mode, combined with evidence of slower offset kinetics and more significant cellular DoA, we chose to pursue **5** as an alternative lead for the program.

Considering **5** as a lead, it already fulfilled our JAK enzyme potency requirements and displayed significant DoA in both enzyme and cellular assays. However, the aqueous solubility of **5** was very poor, to the extent that an accurate measurement could not be determined. In addition, despite a significant increase in lipophilicity compared to the tofacitinib series, turnover in HLM was only modest, where high metabolism was desired. It was however of significant promise that the molecule already contained a phenol group which brought modest turnover in an in vitro assay (HLM UGT) which contained cofactors for phase 2 glucuronidation. Given the apparent importance of the hydrogen bonding interactions of the phenol group in binding to JAK, we postulated that any phase 2 metabolites of the phenol group (for example the glucuronide or sulfate) would be largely inactive as JAK inhibitors, thus greatly reducing any liability from systemic JAK inhibition of potential circulating metabolites. The cross-kinase promiscuity (Figure 4) appeared less optimal for **5**, compared to the tofacitinib chemotype, as it inhibited 9 of 35 additional kinases at the ATP K_m concentration in a screening panel with >50% inhibition at 1 μM compound concentration, although only one of these (ZC1/HGK, also known as MAP4K4) was inhibited at >85%.

Initial structure−activity relationships (Table 3) were investigated around the phenol ring in order to probe for improvements in JAK kinase potency and selectivity, as well as to increase the overall metabolic rate. We employed enzymatic assays for each JAK kinase at 1 mM ATP concentration rather than at the K_m concentrations to gain a better understanding of compound potency and selectivity under more physiologically relevant conditions.[20] In addition assays in primary PBMC cells were used to measure inhibition of the pSTAT5 response to IL-15 for cellular DoA, as well as inhibition of the IFNγ response to IL-2 for potency assessment.

The location of the phenol OH group was shown to be preferred in the para position to the biaryl linkage, as the equivalent meta phenol **6** was a significantly weaker inhibitor against JAK enzymes and in the PBMC cellular assay. This is consistent with the observed X-ray cocrystal structure of **5** where the two hydrogen bonds to the para phenolic OH group appear to be close to optimal distances. Not surprisingly, removal of the OH group or methylation to provide a para methoxyl group resulted in significant loss in potency (data not shown). Increasing the size of the substituent on the phenol ring to either an isopropyl or *n*-propyl group (**7** and **8**) resulted in a drop in both enzyme and cellular potency, while increasing the size of this group still further led to even more significant

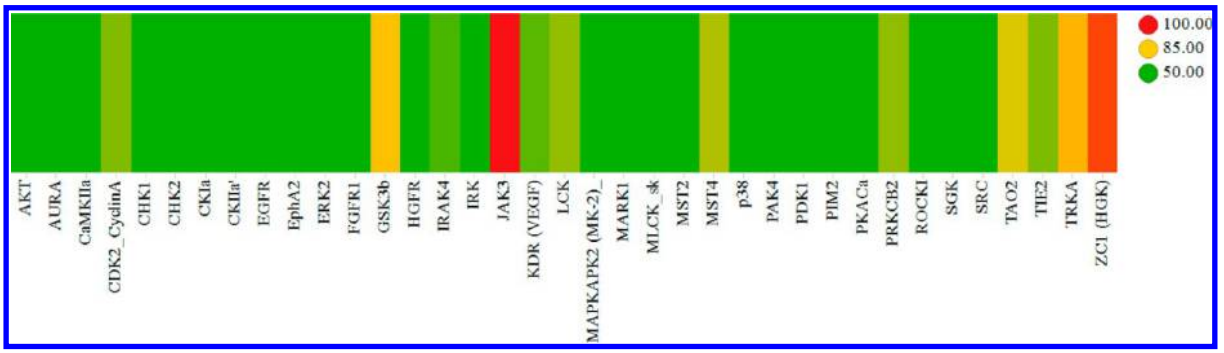

Figure 4. Heat map showing kinase inhibition profile of **5** dosed at 1 μM against a panel of 36 kinases at the ATP K_m concentration. Colors correspond to % inhibition of a given kinase as per the color legend shown.

DOI: 10.1021/acs.jmedchem.6b01634
J. Med. Chem. XXXX, XXX, XXX−XXX

Table 3. SAR around Phenol Ring: JAK Kinase Potency and Selected Cellular Potency Data

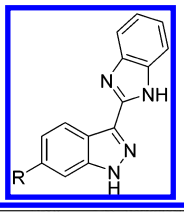

		Enzyme IC_{50} at 1mM ATP (nM)[a]				Cellular IC_{50} (nM)[b]
No.	R	JAK1	JAK2	JAK3	TYK2	PBMC
5	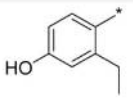	0.4	2.2	8.3	9.1	10.5
6	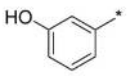	68.6	100.8	493.1	291.2	572.7
7	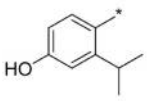	26.8	79.6	293.4	392.3	250.3
8	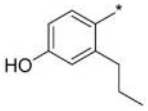	9.7	17.3	166.0	437.5	75.4
9	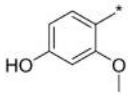	6.1	5.4	43.5	102.1	57.8
10	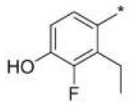	nt	nt	nt	nt	204.8
11	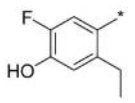	0.8	7.9	16.7	15.3	47.9

[a]Compounds were routinely assayed using Caliper microfluidic assays for their potency of inhibition of phosphorylation of a peptide substrate by the appropriate JAK enzyme at 1 mM ATP concentration. All IC_{50} values reported represent geometric mean values of a minimum of three determinations. nt denotes "not tested". [b]Cellular potency was routinely assayed in peripheral blood mononuclear cells (PBMCs) measuring inhibition of interferon γ (IFNγ) release following stimulation with interleukin 2 (IL2). All IC_{50} values reported represent geometric mean values of a minimum of three determinations.

loss in potency (data now shown). The presence of the ethyl group was found not to be an essential feature for good potency against JAK kinases, as a number of compounds without the ethyl group showed good enzyme and cellular potency. However, these compounds all had far poorer kinase selectivity (data now shown). This suggests that an ethyl substituent is close to the optimal size for a group at this position to maintain good potency while also providing the benefit of improved kinase selectivity. Consistent with this observation, a methoxyl group was also well tolerated at this position, as in **9**, albeit with some loss in potency compared to **5**.

At this point we also explored adding groups such as chloro, cyano, and fluoro adjacent to the phenolic OH group in an attempt to modulate its glucuronidation rate by acidification.[13b] However, to maintain good JAK potency, only fluoro groups were found to be well tolerated in these positions (**10** and **11**), with only a small loss in potency compared to **5**. This is again consistent with the observed binding mode as these positions lie in very close proximity to the protein surface, allowing only for a small atom to be substituted. It appears as though the position para to the ethyl group has slightly more space in the X-ray structure, which is reflected in the better cell potency observed for **11** over **10**. Interestingly, the fluoro substitution para to the ethyl group also resulted in improved kinase selectivity, as **11** inhibited only 3 kinases of a panel of 36 at >50% at 1 μM concentration, with only JAK3 (other JAK family members were not present in the screening subset) in the panel being significantly inhibited at >85% as expected (kinase heat maps for a number of key analogues can be found in the Supporting Information). Gratifyingly, this change also dramatically increased the glucuronidation rate for **11**, which showed a turnover rate in the HLM UGT assay of >360 (μL/min)/mg protein. This was not the case for **10**, which showed no increase in glucuronidation rate (46 (μL/min)/mg protein) versus **5**, despite the two phenols **10** and **11** having very similar calculated pK_a values. Clearly structural effects around the

DOI: 10.1021/acs.jmedchem.6b01634
J. Med. Chem. XXXX, XXX, XXX−XXX

phenol as well as acidification are important contributing factors for overall glucuronidation rates. Fluorophenol **11** also showed good DoA in our cellular wash-out assay, inhibiting the pSTAT5 response with a $T_{1/2}$ of 3.5 h, consistent with the earlier observation for compounds in this series. However, aqueous solubility was again shown to be low and an accurate value could not be measured in a thermodynamic solubility assay. In addition, we could not formulate these molecules successfully for in vivo efficacy evaluation when attempting to use solution dosing via the inhaled route. While indazole-benzimidazoles such as **11** showed some promise to meet our criteria, they were clearly not soluble enough to be considered for dosing via the inhaled route, although useful SAR information had been gained. Moving forward, we needed to address the poor solubility while maintaining the excellent potency and encouraging DoA of this series.

In an attempt to improve compound solubility while maintaining an otherwise favorable profile, we sought to reduce the overall aromatic ring count in our series.[21] SAR investigations in this series were carried out using the nonfluorinated phenol template. Truncating the benzimidazole back to imidazole **12** (Table 4) resulted in no loss of potency in both kinase enzymes and cell based assays. Encouragingly, in addition to excellent potency, we could also see an improvement in thermodynamic solubility (4.1 μM) measured from a crystalline solid sample of **12** in water buffered at pH 7.4. Not surprisingly, truncating further to remove the imidazole completely (R = H) resulted in significant loss of potency given that a key H-bonding interaction with the hinge motif of the kinase had been removed (data not shown). Alternative heterocycles that maintained an H-bonding interaction with the hinge motif, through either an N−H group or aromatic C−H group, in general showed good enzyme inhibition potency but a reduced cellular potency relative to imidazole **12**. Further truncation of the imidazole to the amide functionality, as in primary amide **13** and methylamide **14**, maintained the excellent potency profile while providing a further improvement in solubility (15 μM and 14 μM, respectively, measured from crystalline solid samples in water buffered at pH 7.4). Methylamide **14** in particular showed an excellent kinase selectivity profile with only JAK3 out of a panel of 36 kinases inhibited at >50% at 1 μM concentration. An X-ray cocrystal structure of primary amide **13** binding to JAK2 (Figure 5) showed the expected binding mode for the series, with three key hydrogen bonds in a donor−acceptor−donor motif from the indazole N−H and lone pair and N−H of the amide to the hinge region of the kinase, as well as the two hydrogen bonds from the phenol group to the back pocket residues as noted previously. Not surprisingly, the dimethylamide **15** showed significant loss of potency, consistent with the requirement for the amide N−H hydrogen bonding interaction with the kinase. However, despite adopting the same binding mode as the indazole-benzimidazole **5**, none of these potent and more soluble truncated compounds showed a significant DoA in our cellular assay nor significant slow offset in the kinase kinetic assay. Subsequent compounds that maintained good DoA (vide infra) suggested that additional interactions between the ligand and kinase protein have been lost with this series of smaller amide compounds, leading to the loss of DoA.

We reasoned that further binding potency and improved DoA could be achieved by expanding the amide series into the pocket occupied by the benzimidazole group in our initial lead **5** while maintaining improved solubility. Of a number of larger

Table 4. Replacements for Benzimidazole: JAK Kinase Potency, Cellular Potency and Solubility Data

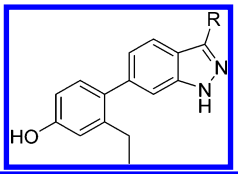

No.	R	Enzyme IC_{50} at 1mM ATP (nM)[a]				Cellular IC_{50} (nM)[b]
		JAK1	JAK2	JAK3	Tyk2	PBMC
5	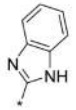	0.4	2.2	8.3	9.1	10.5
12		0.9	0.8	0.8	4.6	10.4
13		1.7	4.2	4.3	54.5	19.1
14		7.5	40.9	125.0	796.2	9.1
15		2756.5	>10000	>10000	>10000	>10000
16	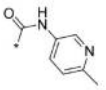	60.0	58.8	418.3	815.9	277.8

[a]Compounds were routinely assayed using Caliper microfluidic assays for their potency of inhibition of phosphorylation of a peptide substrate by the appropriate JAK enzyme at 1 mM ATP concentration. All IC_{50} values reported represent geometric mean values of a minimum of three determinations. [b]Cellular potency was routinely assayed in peripheral blood mononuclear cells (PBMCs) measuring inhibition of interferon γ (IFNγ) release following stimulation with interleukin 2 (IL2). All IC_{50} values reported represent geometric mean values of a minimum of three determinations.

amide analogues prepared, we found that only those made from aromatic amines, for example **16** (Table 4), maintained any reasonable kinase inhibition potency. Upon inspection of the X-ray crystal structure of **16** bound to JAK2 (Figure 5), it is clear that the region of the kinase where the amide heterocyclic group is bound is restricted in size by a triad of surrounding amino acids, Leu-855, Tyr-931, and Gly-935. We found that amides substituted with a methyl group (as in **14**) or a planar group (as in **16**) were tolerated in this position, allowing access through the Leu-Tyr-Gly triad of amino acids to the more open space beyond the hinge region. Heterocyclic amide **16** showed reasonable JAK inhibition potency in both enzymatic and cellular assays, as well as significant DoA in our cellular wash-out assay, with a $T_{1/2}$ of approximately 4.5 h. In addition, kinase selectivity for this compound was good, with only 2 kinases (besides JAK3) in a panel of 36 kinases showing >50% inhibition at 1 μM concentration. Solubility for amide **16**, along with most other larger heterocyclic amides prepared, although improved over **5**, was however found to be poor (0.5 μM). Even though we had reduced the aromatic ring count relative to **5**, amide **16** is still a rather planar molecule where crystal

DOI: 10.1021/acs.jmedchem.6b01634
J. Med. Chem. XXXX, XXX, XXX−XXX

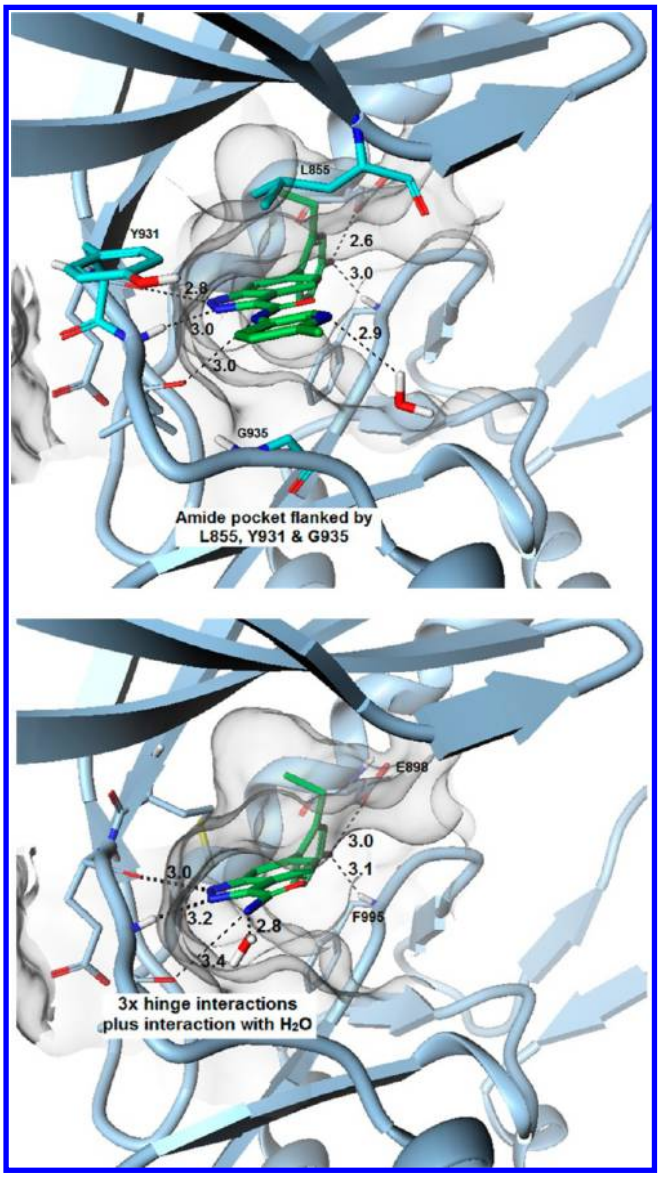

Figure 5. Crystal structures of amides **13** (upper picture, PDB entry 5TQ4) and **16** (lower picture, PDB entry 5TQ5) bound to JAK2. The triad of amino acids restricting exit of more sterically demanding amides from the binding pocket is illustrated in cyan. Numbers correspond to hydrogen bonding distances in angstroms.

packing forces in the solid state are likely to be significant.[22] In addition, chemical stability toward hydrolysis was found to be less than optimal for the majority of these heterocyclic amides over a relatively short time (>10% degradation seen after 1−2 days at pH 8.0 at 40 °C), raising concerns for potential solid form stability and formulation problems in this series. Taken together, these data prompted us to pursue a related but ultimately more successful subseries as described below.

We pursued an alternative tactic to improving solubility while maintaining the overall molecular size and similar shape of the indazole benzimidazole lead, by increasing the sp^3 carbon count in our molecule through saturation of the second aromatic ring of the benzimidazole system.[23] The imidazopiperidine motif **17** (Figure 6) serves this purpose, maintaining the donor−acceptor−donor motif required for hinge binding, as well as the planarity required to maintain binding through the Leu-Tyr-Gly triad of the kinase. In addition, the amine functionality

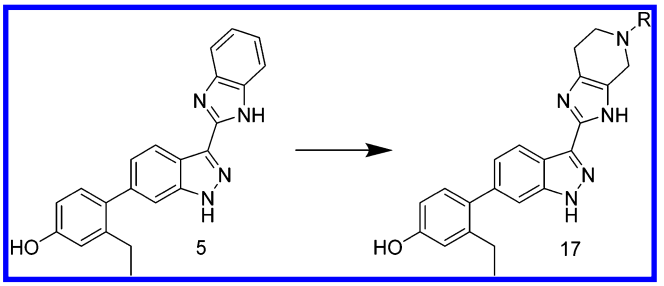

Figure 6. Benzimidazole to imidazopiperidine transformation, showing increasing saturation and sp^3 count in our lead series.

of the piperidine allowed us to further build out from this portion of the molecule to increase binding affinity and DoA.

Our SAR exploration was carried out using both the nonfluorinated and fluorinated (at R2) phenol templates (Table 5). The imidazopiperidine was shown to be an effective replacement for the benzimidazole group in original lead **5**, with amine **18** showing good enzyme and cell potency. Both amide **19** and sulfonamide **20** groups could be prepared with no loss in potency, although the amides typically showed greater cellular potency. This synthetic strategy allowed for a wide range of substituents to be explored, enabling modulation of various properties that could increase HLM and to explore effects on potency, kinase selectivity, and DoA. The methyl and acetamide analogues (**18** and **19**) showed improved solubility over the earlier benzimidazoles as expected (10−20 μM). However, their kinase selectivity profiles were generally much poorer, with at least 10 of a panel of 36 kinases showing >85% inhibition for each of these compounds. Larger substituents, such as benzyl **21** and benzamides **22** and **2**, maintained excellent enzymatic and cellular JAK potency while also introducing significantly higher HLM turnover, in keeping with their increased lipophilicity. We were pleased to find that, as previously discovered, introduction of a fluorine atom para to the ethyl group greatly increased the glucuronidation rate for these compounds. As shown for the fluorinated piperidinyl-pyrazine **2**, the turnover rate in the HLM UGT assay is 129 (μL/min)/mg protein, compared with 17 (μL/min)/mg protein for the nonfluorinated equivalent (compound not shown). These compounds with larger substituents on the piperidine ring also showed significant cellular DoA, typically with $T_{1/2}$ of >6 h.

Fluorinated piperidinyl-pyrazine **2** met all of our in vitro assay criteria and was selected for more advanced studies. Overall it demonstrated good JAK potency, kinase selectivity, metabolic turnover through two different routes of metabolism, as well as sufficient solubility in various formulations for in vivo testing, even though thermodynamic solubility in aqueous solution was low (~0.5 μM). In addition, a crystalline solid form for **2** was found with excellent chemical and physical stability. Most noteworthy, **2** displayed a very long cellular DoA with a $T_{1/2}$ of 9 h in the PBMC cellular wash-out assay. Profiling **2** against a panel of 36 kinases at 1 μM, a concentration that significantly exceeds the JAK cellular and enzymatic IC_{50} values at 1 mM ATP, demonstrated that it has suitable selectivity over non-JAK kinases as only JAK3 was inhibited more than 85% at this concentration (Figure 7).

An X-ray crystal structure of **2** bound to JAK2 (Figure 8) showed the expected binding mode as described previously, with some additional interactions observed with two of the residues flanking the front pocket. First, the piperidinyl-

DOI: 10.1021/acs.jmedchem.6b01634
J. Med. Chem. XXXX, XXX, XXX−XXX

Table 5. Imidazopiperidine Replacement for Benzimidazole: JAK Kinase Potency and Selected Cellular Potency Data

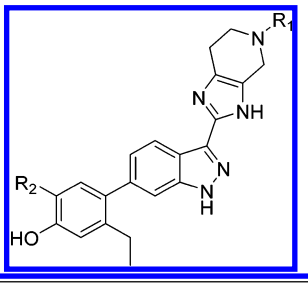

			Enzyme IC_{50} at 1mM ATP (nM)[a]				Cellular IC_{50} (nM)[b]	Microsomal clearance assays (μL/min/mg protein)	
No.	R1	R2	JAK 1	JAK 2	JAK 3	TYK 2	PBMC	HLM[c]	HLM UGT[d]
18		H	2.1	6.4	2.9	20.1	18.6	56	<1.9
19		H	0.5	3.3	7.1	22.7	4.5	42	5.5
20		H	1.3	5.6	1.3	25.1	39.1	18	7.3
21	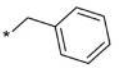	F	1.8	15.9	31.0	57.5	30.4	75	>360
22	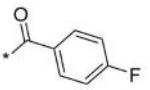	F	<0.1	0.3	1.7	0.8	35.0	48	37
2	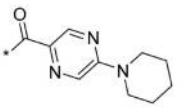	F	2.2	23.1	59.9	29.7	70.3	101	129

[a]Compounds were routinely assayed using Caliper microfluidic assays for their potency of inhibition of phosphorylation of a peptide substrate by the appropriate JAK enzyme at 1 mM ATP concentration. All IC_{50} values reported represent geometric mean values of a minimum of three determinations. [b]Cellular potency was routinely assayed in peripheral blood mononuclear cells (PBMCs) measuring inhibition of interferon γ (IFNγ) release following stimulation with interleukin 2 (IL2). All IC_{50} values reported represent geometric mean values of a minimum of three determinations [c]Compounds were routinely assessed for metabolic stability in human liver microsomes (HLMs). [d]Compounds were assessed for phase II glucuronidation in HLM by including the microsomal activator Brij58 and cofactor uridine diphosphate glucuronic acid (UDPGA) and excluding the cytochrome P450 dependent cofactor NADPH.

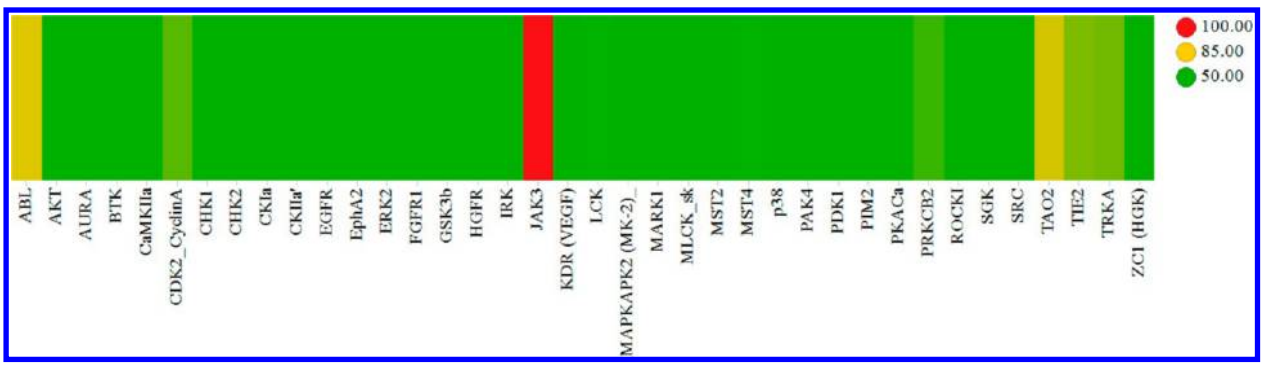

Figure 7. Heat map showing kinase inhibition profile of **2** dosed at 1 μM against a panel of 36 kinases. Colors correspond to % inhibition of a given kinase as per the color legend shown.

DOI: 10.1021/acs.jmedchem.6b01634
J. Med. Chem. XXXX, XXX, XXX−XXX

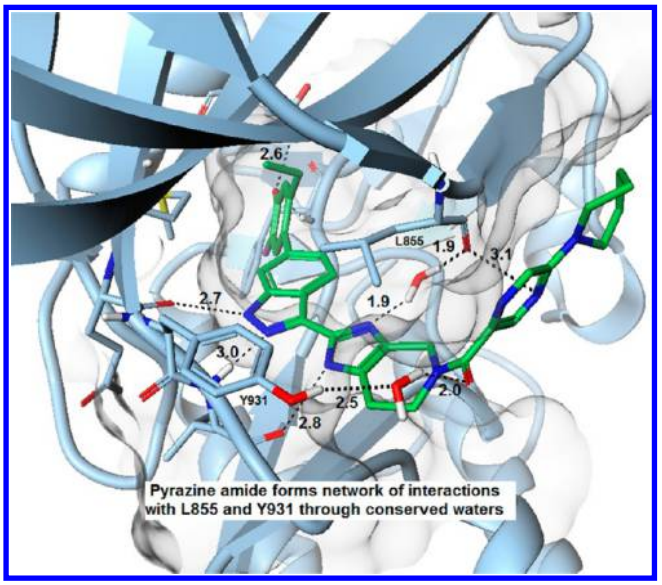

Figure 8. X-ray cocrystal structure of **2** bound to JAK2 (PDB entry 5TQ8).

pyrazine heterocyclic moiety is wrapped alongside and engaged in a π-stacking interaction with the amide carbonyl groups of Leu-855 in the glycine rich P-loop, which also bridges through water to interact with the imidazole ring. Second, the amide carbonyl in **2** bridges via another conserved water to interact with Tyr-931. This additional network of binding interactions might explain the longer DoA observed with this larger class of compound within this series.

JAK Inhibitory Profile of 2 in Human Whole Blood (HWB). In order to test functional potency and to provide insight into the JAK inhibitory profile of **2**, studies in human whole blood investigated inhibition of STAT phosphorylation induced by a selection of cytokines known to signal through various combinations of JAK enzymes (Table 6). In each assay

Table 6. Inhibitory Potency of 2 in Human Whole Blood versus Various Stimulatory Cytokines

cytokine	JAK dimer	white blood cells	pSTAT	IC_{50} (μM)[a]	free IC_{50} (nM)
IFNα	JAK1/TYK2	lymphocytes	pSTAT3	0.62	0.62
IL-23	JAK2/TYK2	lymphocytes	pSTAT3	4.2	4.2
IL-4	JAK1/JAK3	monocytes	pSTAT6	1.8	1.8
IL-6	JAK1/JAK2	monocytes	pSTAT3	2.1	2.1
GM-CSF	JAK2/JAK2	monocytes	pSTAT5	5.2	5.2

[a]All IC_{50} values reported represent geometric mean values of a minimum of three determinations.

the inhibition by **2** of STAT phosphorylation was measured in a specific subpopulation of white blood cells and IC_{50} values were determined. Free IC_{50} values were calculated by taking into account plasma protein binding, where the fraction unbound in plasma is 0.001. These data confirmed that **2** is a functional pan-JAK inhibitor in human whole blood.

Pharmaceutical Properties of 2. Fluorinated piperidinyl-pyrazine **2** is a lipophilic compound with a cLogP of 4.4 and log *D* of 3.9 (measured by a shake flask method). The molecular weight of the compound is 566 Da, and the topological polar surface area (TPSA) is calculated to be 126 Å^2. The compound contains both a weakly basic imidazole group with a measured pK_a of 4.5 and a weakly acidic fluorophenol group with a measured pK_a of 8.7. Following extensive screening efforts, including efforts to generate various salt forms of the compound, a stable neutral nonsolvated crystalline form was found that could be crystallized directly from the final reaction step to provide a means of isolating the compound with excellent purity (Figure 9, left-hand panel). This form has very low hygroscopicity and is chemically stable both at room temperature and at 40 °C with 75% relative humidity for up to 6 weeks, underwriting its long-term stability. The material is also stable to jet milling to provide solid material with regular and consistent particle size in the respirable range (~2 μm).[24] The resulting micronized material (Figure 9, right-hand panel) has been found to be chemically and physically stable when blended with lactose for up to 4 weeks, demonstrating its suitability for use in a dry powder inhalation device.

In addition this crystalline material was also amenable to preparation as a 4% solution in a base formulation typically used in topical applications to the skin as shown in Table 7.

In Vitro Metabolism and Pharmacokinetic Properties of 2. Following in vitro incubation of **2** in human hepatocytes, the major metabolites observed were produced by direct glucuronidation and P450 metabolism, consistent with the presence of the fluorinated phenol group functioning as an effective handle for phase II conjugation. As discussed previously in relation to the binding mode of **2**, these phenol conjugated metabolites are expected to show no inhibition of JAK kinases once formed. This metabolic profile was consistent across rat and dog in in vitro hepatocyte and microsomal metabolism studies.

The pharmacokinetic properties of **2** were assessed in vivo and were found to be consistent with its high lipophilicity and neutral physicochemistry (Table 8). Consistent with the high in vitro intrinsic clearance values previously described, **2** exhibits very high unbound clearance in the rat and dog and has an oral bioavailability of <5% following oral solution administration to the rat.

On the basis of these human in vitro data and the in vivo rat and dog pharmacokinetic data, **2** was predicted to be cleared in humans by glucuronidation and CYP3A4 metabolism, exhibiting low levels of unbound circulating parent following inhaled or dermal delivery due to high unbound clearance. Due to the predicted negligible oral absorption and lack of observed circulating metabolites in animal Pk studies, the potential for significant levels of circulating active metabolites in human was deemed to be low risk. Therefore, following topical dosing to either the lung or skin, **2** demonstrated suitable pharmacokinetic properties to provide high confidence that it would demonstrate an organ targeted effect, with negligible systemic exposure of parent compound and no active circulating metabolites. On the basis of the multiple routes of metabolism (P450 and glucironidation) and projected low levels of unbound exposure in human, the potential for **2** to be either a victim or perpetrator of a drug−drug interaction was also deemed to be low.

Biological in Vivo Activity of 2. The in vivo activity of **2** dosed as a solution via the intratracheal (i.t.) route was demonstrated in a mouse pharmacodynamic model of IL-6 induced pSTAT3 response in the lungs, mediated via the JAK1/JAK2 mechanism (Figure 10). **2** caused a dose-related inhibition of the IL-6-elicited increase in lung pSTAT3, giving an ED_{50} of approximately 3 μg/animal. For comparison, the

DOI: 10.1021/acs.jmedchem.6b01634
J. Med. Chem. XXXX, XXX, XXX−XXX

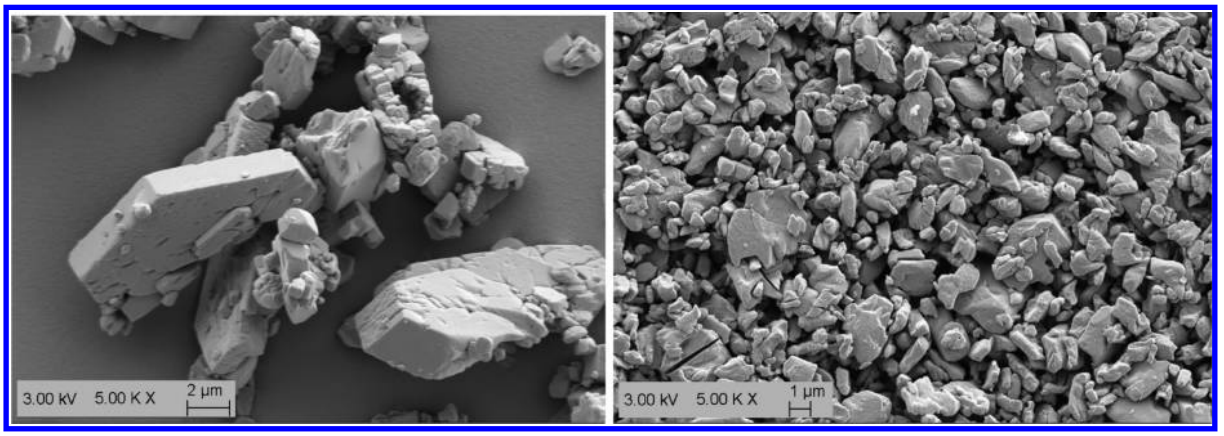

Figure 9. SEM images of solid **2** following crystallization (left-hand panel) and subsequent micronization (right-hand panel).

Table 7. Components of 4% Dermal Formulation of 2

component	% wt/wt
2	4
propylene glycol	30
polyethylene glycol 400	30
dimethyl isosorbide	10
glycerin	25.9
BHA	0.1

inhaled corticosteroid, fluticasone propionate, demonstrates an ED_{50} of between 3 μg/animal and 30 μg/animal across a variety of mouse models when dosed i.t.

In vivo activity was also assessed via topical application of **2** to the skin of a mouse ear in a dermal model of IL-23 induced inflammation (Figure 11). IL-23 is known to be a major driver of psoriasis pathology mediated via the JAK-STAT pathway.[25] For mice ears treated topically with **2** as a 4% solution, a significant reduction of ear swelling (48%) was observed over a period of 11 days following multiple IL-23 injections in the ear, consistent with inhibition of the JAK2/TYK2 pathway. For compound treated mice, swelling typically occurred to less than 50 μm, while ears of control mice receiving IL-23 injections with no compound treatment typically swelled to over 100 μm.

Proof of organ targeted JAK inhibition in the lung versus systemic JAK inhibition was shown by comparison of lung pSTAT3 inhibition to systemic pSTAT5 inhibition following i.t. dosing of **2** (Figure 12). **2** inhibited phosphorylation of STAT3 in the lung following IL-6 stimulation by 100% at doses of 10 μg and above. In contrast, a 10 μg dose resulted in no inhibition of STAT5 phosphorylation in the blood following ex vivo GM-CSF stimulation, while a 100 μg resulted in less than 50% inhibition. These data provide evidence that **2** exerts significantly greater efficacy in the lung compared to within the blood following i.t. administration, and this is consistent with very low systemic exposures expected when considering the pharmacokinetic properties of **2**.

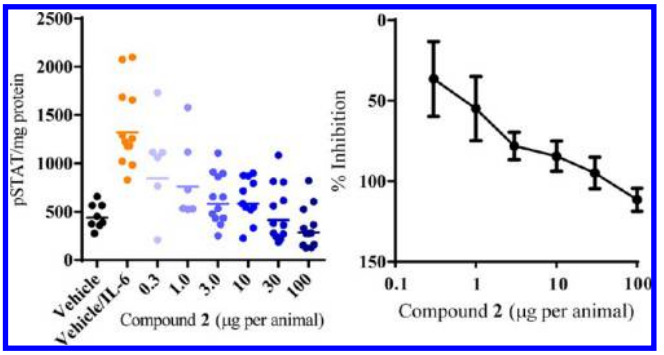

Figure 10. Effects of intratracheal administration of **2** on IL-6 (i.t.) induced increases in lung phosphorylated STAT3 in the mouse. Left hand panel represents absolute quantity of phosphorylated pSTAT in mouse lung. Right hand panel represents the percentage inhibition ± 95% CI calculated from the difference in geometric mean values between vehicle/IL-6-treated and vehicle/saline-treated groups.

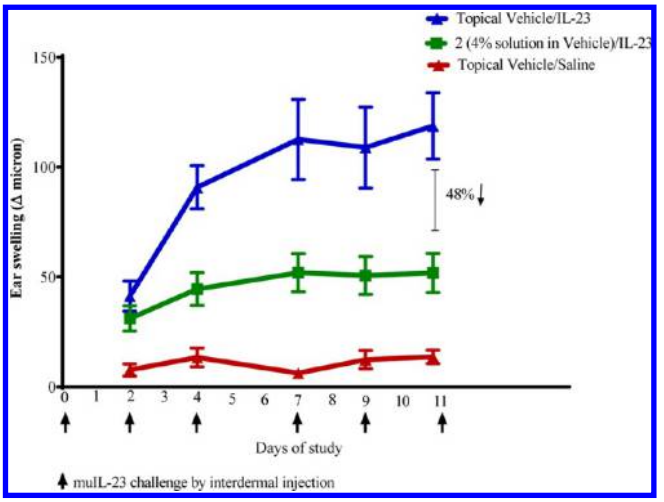

Figure 11. Effects on mouse ear swelling following IL-23 injection and treatment with a topical formulation of **2**.

Table 8. In Vivo Rat and Dog Plasma Pharmacokinetic Data of 2 after Intravenous (iv) and Oral (po Dosing

species	dose (mg/kg)	Cl (mL min^{-1} kg^{-1})	$Cl_{unbound}$ [c] (mL min^{-1} kg^{-1})	V_{ss} [b] (L/kg)	terminal $T_{1/2}$ [b] (h)	oral bioavailability (%)
rat iv	0.5	48	>48000	0.8	2.1	
rat po	1					<5
dog iv	0.1[a]	18	>18000	1.0	2.0	

[a]30 min infusion. [b]Parameters from iv PK profile. [c]Plasma protein binding, ≥99.9%.

DOI: 10.1021/acs.jmedchem.6b01634
J. Med. Chem. XXXX, XXX, XXX−XXX

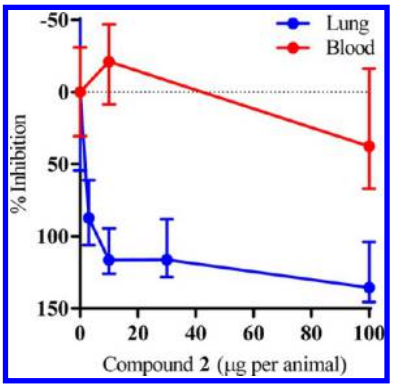

Figure 12. Effects of i.t. administration of **2** on inhibition of STAT phosphorylation in the lungs and blood. Data show the effect on IL-6-induced lung phosphorylated STAT3 or GM-CSF-induced blood phosphorylated STAT5 with values representing the percentage inhibition ± 95% CI calculated from the difference in geometric mean values between vehicle/IL-6-treated and vehicle/saline-treated groups: N = 6 (lung) and N = 3 (blood).

Sustained occupancy of JAK1 after i.t. dosing was also demonstrated in this model, supporting the potential for an extended DoA in human lung. The JAK1 occupancy of **2** in mouse lung was measured by ActivX Biosciences, Inc. (San Diego, CA, U.S.) following i.t. administration of either 10 μg (ED_{80} dose) or 100 μg (maximum inhibitory dose tested) of **2**.[26] These data suggest that **2** maintains significant target occupancy 4 h postdose for JAK1 (Figure 13), which is

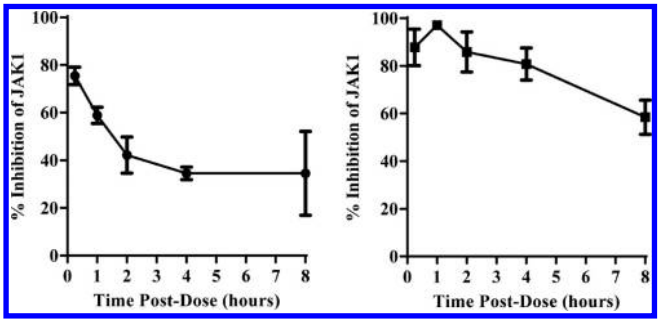

Figure 13. Effects of i.t. administration of **2** on JAK1 target occupancy. Values represent the % occupancy over time with a dose of 10 μg (left-hand graph) or 100 μg (right-hand graph).

consistent with the long duration of action demonstrated in human in vitro cell systems. Given that the half-lives of JAK enzymes in cellular systems have previously been determined to be 2−3 h,[27] the long duration of action that we observe could be by virtue of tissue retention of the compound in the mouse lung in the in vivo assays, as well as cellular retention of compounds in the in vitro assays, in addition to compound kinetic slow-off effects on the kinase.

In Vitro and in Vivo Safety Profile of 2. **2** was screened at 10 μM in a panel of receptors, transporters, enzymes, and ion channels (CEREP radioligand binding and enzyme inhibition profile), which demonstrated greater than 50% inhibition of binding or activity against a small number of targets, namely, 5-HT_7, Abl kinase, acetylcholinesterase, α_{2B} adrenergic receptor, AurA/Aur2 kinase, KDR kinase, Lck kinase, and Na^+ channel (site 2). However, these activities were observed at multiples of greater than 100-fold above the projected free systemic plasma exposures at the maximum clinical lung dose (200 μg), so **2** was not anticipated to have any consequences at these receptors, transporters, enzymes, and ion channels if evaluated at clinically relevant exposures. Furthermore, **2** had no effects on the hERG potassium current at 1 μM (<1% inhibition). Cough has historically been a major cause of attrition of inhaled therapies, so **2** was dosed up to 2 mg in 400 μL of micelle vehicle to the mouse A delta fiber sensory nerve preparation. No nerve activation was detected with **2**, providing evidence that **2** presents a low risk for cough effects. Exploratory 7-day intravenous toxicology studies were conducted in rats and dogs to assess risk associated with systemic exposure. There were no adverse test article-related findings in any of the parameters evaluated, with a 36-fold margin achieved in rat over total plasma AUC based on a projected exposure following a human clinical lung dose of 200 μg, and a 55-fold margin achieved in dog plasma AUC. The BioLum Ames bacterial mutagenicity assay showed no evidence of genetic toxicity with and without metabolic activation, which was also the case for the CHO in vitro micronucleus test. Peripheral blood micronucleus assessment was also made from the rat 7-day intravenous exploratory toxicology study, and no evidence of genetic toxicity was observed.

Chemistry: Synthesis of Compounds. The tofacitinib analogue with phenolic sulfone **4** was prepared as detailed in Scheme 1, beginning with alcohol **23**, whose preparation has been detailed previously.[3a] Reaction of the secondary alcohol with disulfanediyldiphenol proceeded with inversion of stereochemistry, providing the sulfide **24**, which was oxidized with potassium peroxymonosulfate to sulfone **4**.

Our lead indazole **5** and initial indazole analogues **6** and **9** were available in the Pfizer compound collection having been prepared earlier according to procedures outlined in the patent literature.[18]

The synthetic strategy for preparation of the majority of the indazoles is outlined in Scheme 2. The key reaction involved formation of a biaryl bond through palladium-catalyzed cross coupling of indazoles **h** with protected phenols **g** to provide key

Scheme 1. Synthesis of Tofacitinib Analogues[a]

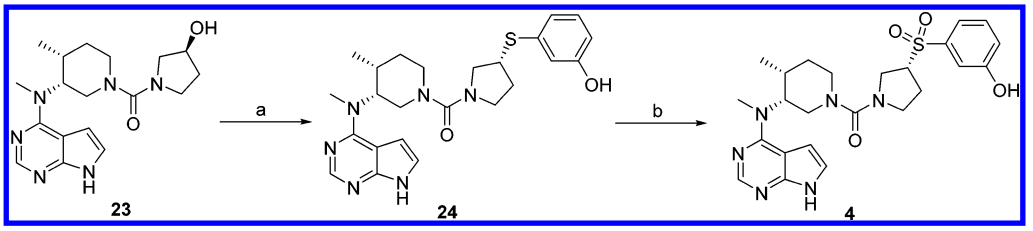

[a]Reagents and conditions: (a) 3,3′-disulfanediyldiphenol, Bu_3P, toluene, 100 °C, 3 h, 69%; (b) potassium peroxymonosulfate, H_2O, THF, IPA, rt, 1 h, 95%.

DOI: 10.1021/acs.jmedchem.6b01634
J. Med. Chem. XXXX, XXX, XXX−XXX

Scheme 2. Retrosynthesis for Preparation of Target Indazoles

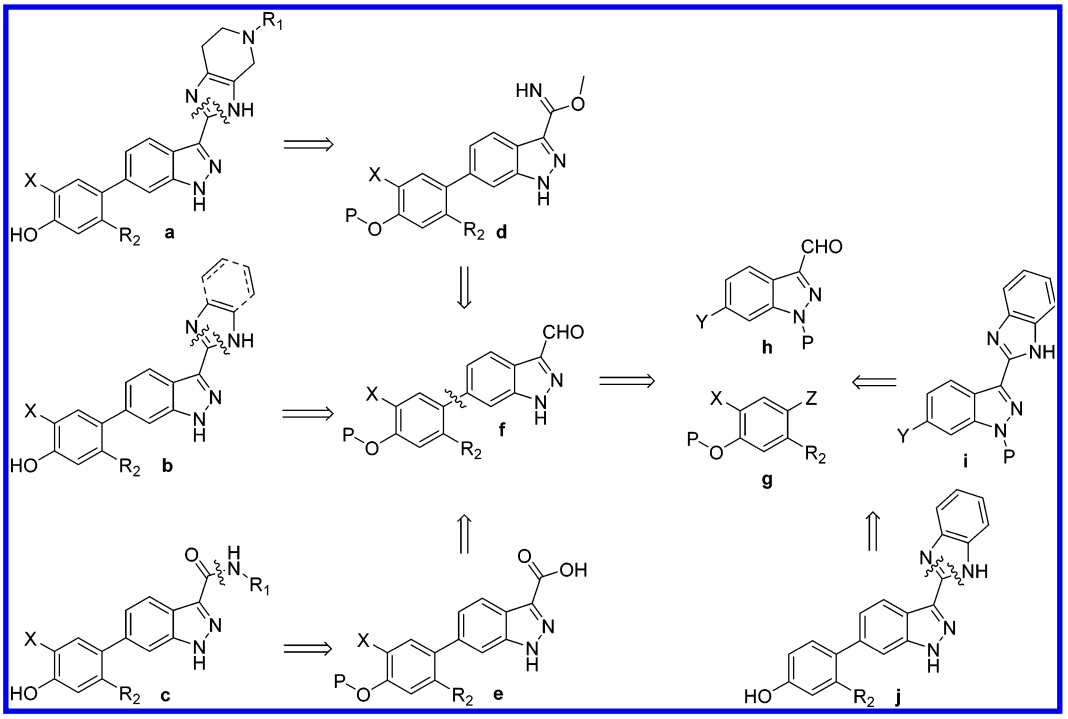

Scheme 3. Synthesis of Indazoles[a]

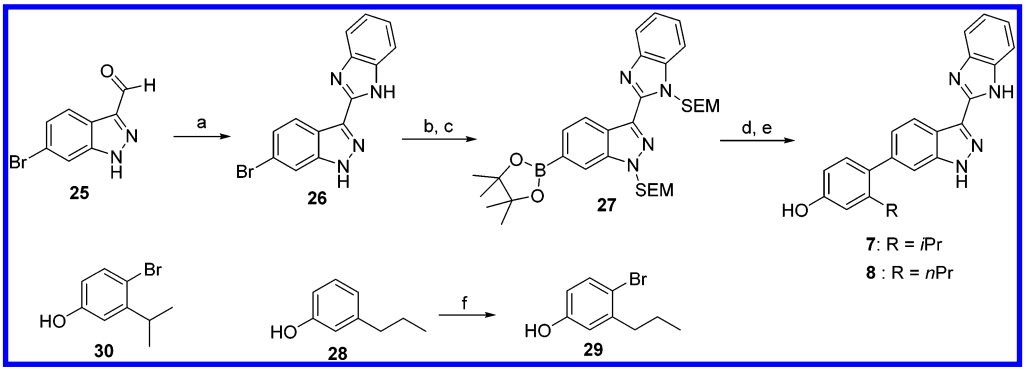

[a]Reagents and conditions: (a) benzene-1,2-diamine, NH_4Br, MeOH, 0 °C to rt, 18 h, 52%; (b) NaH, THF, 0 °C, 30 min, then (2-trimethylsilyl)ethoxymethyl chloride, 2 h, 58%; (c) bis(pinacolato)diboron, (dppf)$PdCl_2$, KOAc, 1,4-dioxane, 100 °C, 15 h, 97%; (d) 4-bromo-3-(propan-2-yl)phenol **30** or 4-bromo-3-propylphenol **29**, $PdCl_2(PPh_3)_2$, Na_2CO_3, DME, 150 °C, 1 h, 22−30%; (e) conc HCl, MeOH, 60 °C, 18 h, 56−88%; (f) NBS, MeCN, 0 °C to rt, 18 h, 84%.

intermediate biaryl indazolo-aldehydes **f**, through which the majority of targets were prepared. The aldehyde functionality in **f** could be directly reacted with diamines to provide imidazole analogues **b** or converted to either imidates **d** or carboxylic acids **e**. Imidazopiperidine targets **a** could be accessed from the imidate intermediate **d**, while amide targets **c** could be accessed from the carboxylic acid **e**. For certain targets **j**, the aldehyde functionality in **h** was first converted to a benzimidazole providing **i**, before palladium catalyzed cross coupling with phenols **g**.

The propyl substituted indazolophenols **7** and **8** were prepared as detailed in Scheme 3. The aldehyde group of bromoindazole **25** was first converted to a benzimidazole group through reaction with 1,2 diaminobenzene and ammonium bromide providing **26**. Following SEM protection of the N−H groups, the bromide was converted to a boronic ester affording **27** in good yield. Following bromination of the phenol **28**, the resulting bromide **29**, or the commercially available bromide **30**, was reacted with **27** in a palladium catalyzed cross-coupling reaction to provide the final targets **7** and **8** in reasonable yield.

The fluorophenol containing targets **10** and **11** were prepared in a similar manner as detailed in Scheme 4. We found it preferable to reverse the polarity of the Pd-coupling to install the boronic ester on the protected phenol portion of the molecule first while maintaining the bromide on the indazole ring. This arrangement of required reaction partners generally provided improved yields in the subsequent palladium catalyzed cross-coupling reaction over the earlier route described in Scheme 3. Bromination of commercially available fluoromethoxybenzenes **31** and **32** followed by boronic ester formation provided the boronic esters **33** and **34**. Cross-coupling with bromoindazole **25** then provided aldehydes **35** and **36**. Reaction of the aldehyde group with 1,2 diamino-benzene and sodium sulfite provided the corresponding

DOI: 10.1021/acs.jmedchem.6b01634
J. Med. Chem. XXXX, XXX, XXX−XXX

Scheme 4[a]

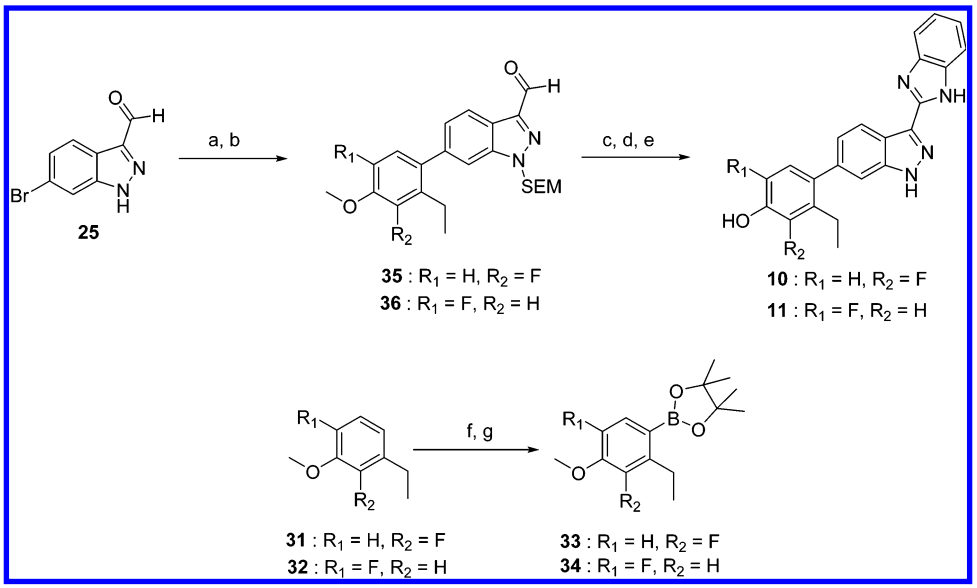

[a]Reagents: (a) NaH, THF, 0 °C 1 h, then (2-trimethylsilyl)ethoxymethyl chloride, 0 °C to rt, 16 h, 99%; (b) **33** or **34**, $(Ph_3P)_4Pd$, K_3PO_4, 1,4-dioxane, H_2O, 100 °C, 15 h, 68−71%; (c) benzene-1,2-diamine, Na_2SO_3, DMA, 100 °C 16 h, 65−70%; (d) conc HCl, MeOH, 60 °C, 16 h, 80−82%; (e) BBr_3, DCM, rt, 72 h, 20−54%; (f) NBS, MeCN, 0 °C to rt, 18 h; (g) bis(pinacolato)diboron, $(Ph_3P)_4Pd$, K_3PO_4, 1,4-dioxane, 100 °C, 15 h, 33−38% over 2 steps.

Scheme 5[a]

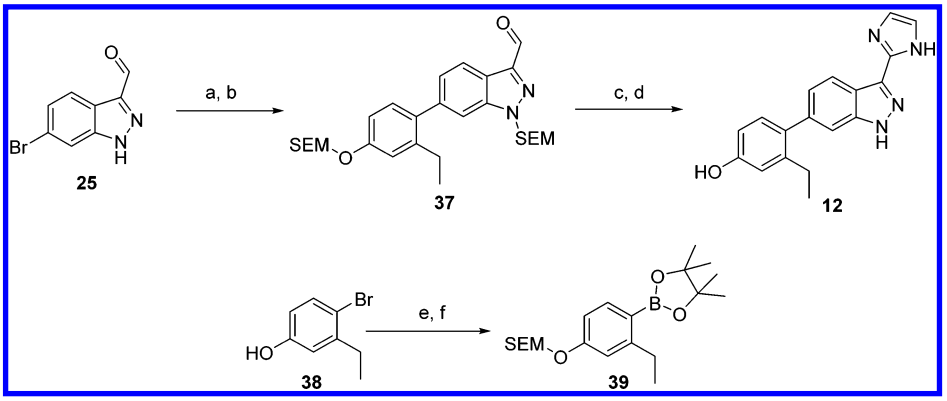

[a]Reagents: (a) NaH, THF, 0 °C 1 h, then (2-trimethylsilyl)ethoxymethyl chloride, 0 °C to rt, 16 h, 99%; (b) **39**, $(Ph_3P)_4Pd$, K_3PO_4, 1,4-dioxane, H_2O, 100 °C, 16 h, 94%; (c) glyoxal, NH_4OH, MeOH, THF, rt, 16 h, 18%; (d) TBAF, THF, 1,2-diaminoethane, 80 °C, 16 h, 35%; (e) (2-trimethylsilyl)ethoxymethyl chloride, DIEA, DCM, rt, 18 h, 83%; (f) bis(pinacolato)diboron, $(Ph_3P)_4Pd$, K_3PO_4, 1,4-dioxane, 100 °C, 16 h, 21%.

benzimidazoles which were processed to the final targets **10** and **11** by removal of the SEM group and deprotection of the methyl ether.

The imidazole **12** was prepared as shown in Scheme 5. We found in general a SEM to be a convenient protecting group for the phenol, allowing for a more straightforward and unified final deprotection step as compared to a methyl ether. Thus, the phenol in commercially available aryl bromide **38** was protected with a SEM group before conversion of the bromide to a boronic ester, providing **39**. Cross-coupling with bromoindazole **25** proceeded in excellent yield to give aldehyde **37**. Conversion of the aldehyde to an imidazole group with glyoxal and ammonium hydroxide followed by removal of the SEM groups provided the final target imidazole **12**.

Amides **13**−**16** were prepared as detailed in Scheme 6. Aldehyde **37** was either oxidized, providing the corresponding carboxylic acid **40** following removal of the SEM groups, or converted to the nitrile **41** via dehydration of the corresponding oxime. Standard amide bond forming reactions with the acid **40** provided secondary and tertiary amides **14**−**16**, while the nitrile **41** was treated with basic hydrogen peroxide to provide the primary amide **13** following SEM group removal.

Our initial synthesis of imidazopiperidine analogues such as **18**−**20** involved a key palladium catalyzed Stille cross-coupling reaction between the protected iodoimidazopiperidine **46**, prepared from commercially available imidazopiperidine **45**, and the trimethylstannate derived from iodide **43**, which itself derived from iodoindazole **42** through cross coupling with boronate ester **39** followed by iodination and SEM protection (Scheme 7). The Stille cross coupling reaction proceeded in low to moderate yield to provide the indazole-imidazopiperidine **44** following global deprotection. The free amine group of the unprotected piperidine could then be used successfully in reductive amination chemistry, amide and sulfonamide bond formation, providing analogues **18**−**20**.

DOI: 10.1021/acs.jmedchem.6b01634
J. Med. Chem. XXXX, XXX, XXX−XXX

Scheme 6[a]

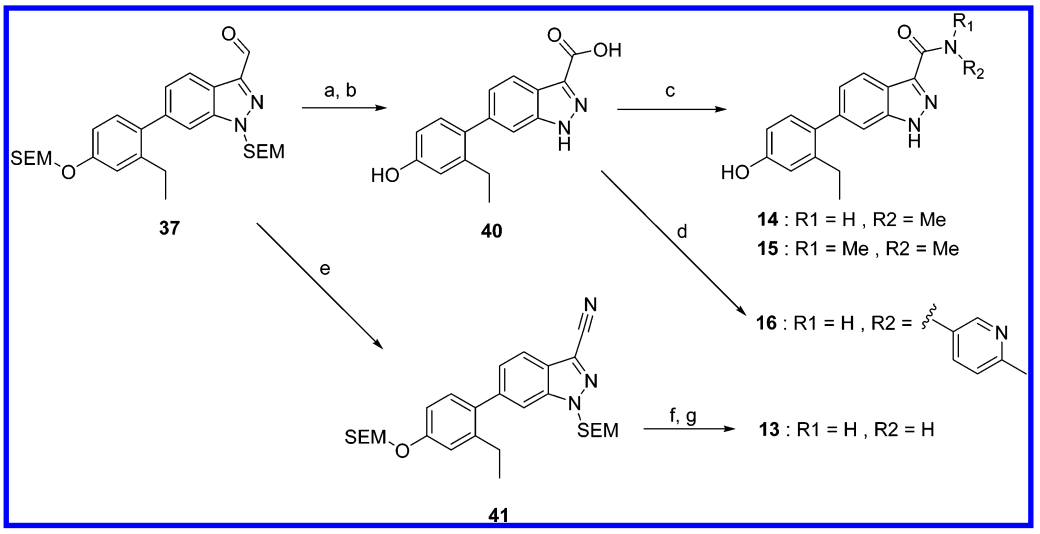

[a]Reagents and conditions: (a) $NaClO_2$, 2-methylbut-2-ene, NaH_2PO_4, ^tBuOH, H_2O, rt, 1 h, 72%; (b) TBAF, THF, 1,2-diaminoethane, rt, 16 h, 41%; (c) methylamine or dimethylamine hydrochloride, EDC, HOBT, 4-methylmorpholine, DMF, rt, 16 h, 60−63%; (d) 2-methyl-5-aminopyridine, HATU, TEA, DMAP, DMA, 30 °C, 16 h; (e) (i) hydroxylamine hydrochloride, Et_3N, MeCN, 60 °C, 1.5 h; (ii) trichloroacetyl chloride, Et_3N, MeCN, 60 °C, 16 h, 82%; (f) 30% H_2O_2, KOH, EtOH, rt, 4 h, 82%; (g) TBAF, THF, 1,2-diaminoethane, 60 °C, 3 h, 63%.

Scheme 7[a]

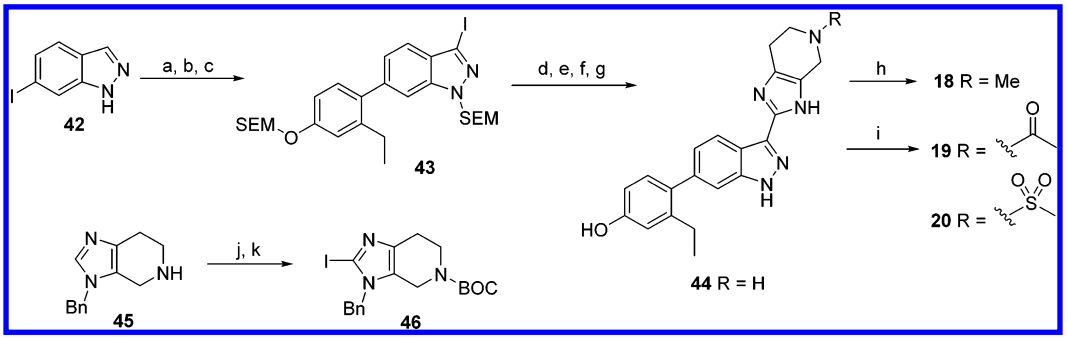

[a]Reagents: (a) **39**, (dppf)$PdCl_2$, K_3PO_4, DME, H_2O, 140 °C, 1 h, 79%; (b) KOH, DMF, rt, 5 min, then I_2, rt, 30 min, 84%; (c) NaH, THF, 0 °C 15 min, then (2-trimethylsilyl)ethoxymethyl chloride, 0 °C to rt, 16 h, 40%; (d) $(Me_3Sn)_2$, $(Ph_3P)_4Pd$, toluene, 80 °C, 16 h, 69%; (e) **46**, CuI, $(Ph_3P)_4Pd$, THF, 65 °C, 90 h, 26%; (f) $Pd(OH)_2/C$, H_2 200 psi, EtOH, 60 °C, 24 h, 86%; (g) conc HCl, MeOH, 64 °C, 18 h, 100%; (h) CH_2O 37% in H_2O, $NaBH(OAc)_3$, DIEA, DMF, AcOH, rt, 16 h, 50%; (i) Ac_2O or $(MeSO_2)_2O$, Et_3N, DMF, rt, 16 h, 13−30%; (j) Boc_2O, Et_3N, DCM, 0 °C to rt, 16 h, 85%; (k) *n*-BuLi, THF, −78 °C, then I_2, 1.25 h, 33%.

An alternative synthetic route (Scheme 8) was used to prepare additional imidazopiperidine analogues such as **21**, which involved a condensation reaction between imidate **48** and amino acetal **53**, followed by cyclocondensation of amidine intermediate **49**. This route provided a facile and more reliable route to key targets, providing significantly higher yields on scale up and avoiding the use of tin reagents on larger scale. Imidate **48** was prepared from the commercially available bromoindazole **25** through initial THP protection and conversion of the aldehyde to a nitrile group, providing **47**. Palladium catalyzed cross-coupling with the boronate ester **51** and conversion of the nitrile to an imidate using sodium methoxide furnished **48**. The boronate ester itself was prepared from commercially available fluorophenol **50**, which was first brominated in the position para to the phenol, followed by SEM protection of the phenol and palladium catalyzed boronate ester formation, providing **51**. The requisite amino acetal **53** was prepared according to a known sequence from commercially available 4-ketopiperidine **52**, a key step in the sequence being a Neber rearrangement.[28] Following condensation of imidate **48** and amino acetal **53**, cyclocondensation of the amidine **49** was carried out under acidic conditions which also led to successful deprotection of the SEM and THP groups, providing target amine **21** in excellent yield.

In order to prepare further amide derivatives of the imidazopiperidine group, as well as to provide a more unified and efficient protecting group strategy, we employed the Boc protected amino acetal **57** in the condensation reaction with imidate **48** (Scheme 9). Treatment of the resulting amidine **54** with acid led to cyclocondensation and global deprotection of all acid labile protecting groups, providing imidazopiperidine **55** in excellent overall yield. The amino acetal **57** was prepared according to a known sequence involving a Neber rearrangement from commercially available 4-ketopiperidine **56**.[29] Intermediate **55** was a highly versatile intermediate that could be prepared on multigram scale following the synthetic procedures described herein. The piperidine amino group could be reacted selectively to prepare a range of amides, sulfonamides, carbamates, ureas, and tertiary amines. Synthesis

DOI: 10.1021/acs.jmedchem.6b01634
J. Med. Chem. XXXX, XXX, XXX−XXX

Scheme 8[a]

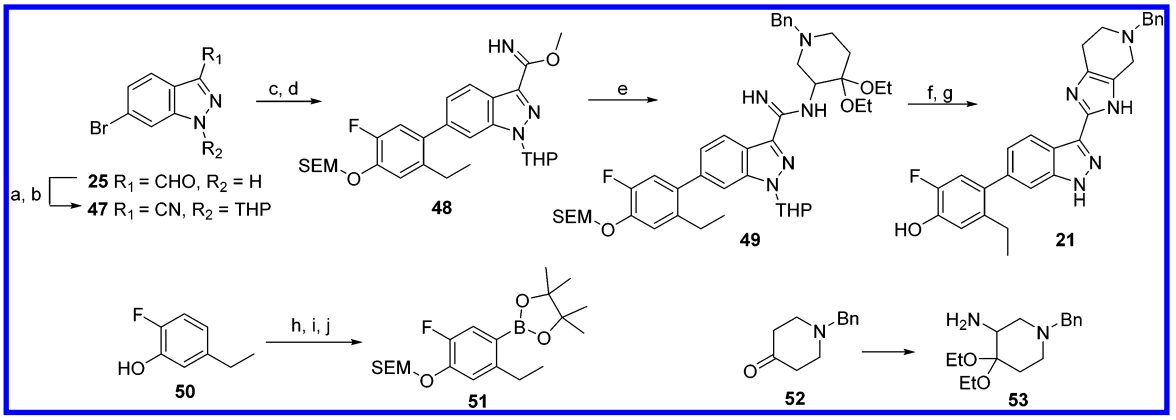

[a]Reagents and conditions: (a) 3,4-dihydro-2*H*-pyran, pTSA, DCM, 0 °C to rt, 16 h, 73%; (b) hydroxylamine hydrochloride, Et_3N, MeCN, 60 °C, 3 h, then TFAA, Et_3N, MeCN, 0 °C to rt, 2 h, 99%; (c) **51**, $(Ph_3P)_4Pd$, K_3PO_4, 1,4-dioxane, H_2O, 110 °C, 18 h, 81%; (d) NaOMe, MeOH, rt, 18 h, 100%; (e) **53**, AcOH, EtOH, 50 °C, 18 h, 45%; (f) conc HCl, EtOH, rt, 18 h, 100%; (g) conc HCl, EtOH, 65 °C, 18 h, 80%; (h) $CuBr_2$, MeCN, rt, 16 h, 100%; (i) (2-trimethylsilyl)ethoxymethyl chloride, DIEA, DCM, rt, 18 h, 86%; (j) bis(pinacolato)diboron, $Pd(dppf)Cl_2$, KOAc, 1,4-dioxane, 100 °C, 18 h, 100%.

Scheme 9[a]

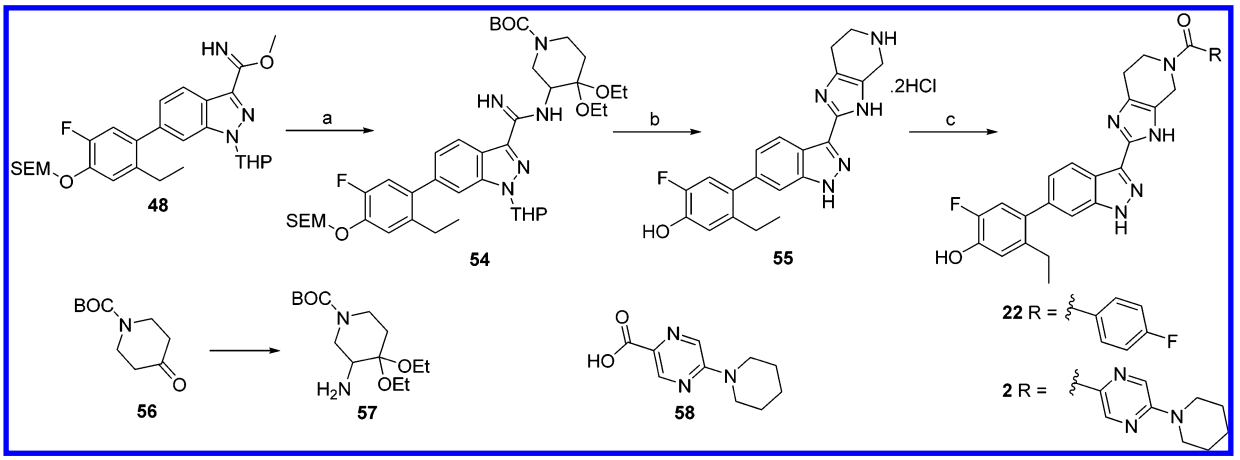

[a]Reagents and conditions: (a) **57**, AcOH, EtOH, 50 °C, 18 h, 100%; (b) conc HCl, EtOH, rt, 18 h, 88%; (c) 4-fluorobenzoic acid or **58**, HATU, DIEA, DMF, rt, 18 h, 89%;

of two key amide analogues is illustrated in Scheme 9. Standard amide bond coupling conditions using HATU were employed to couple **55** with commercially available parafluorobenzoic acid or pyrazine carboxylic acid **58**, providing amides **22** and **2** in excellent yields.

CONCLUSIONS

We have described our approach to the discovery of a novel JAK inhibitor **2** that is well suited for inhaled delivery to the lungs and/or topical delivery to the skin. Our initial effort to work within our clinically precedented tofacitinib chemical series produced compounds that met most of the requirements for our program, but these did not have the key fundamental property of DoA. This led us to adopt a new approach and use X-ray crystal structures to guide a targeted screening effort to find JAK inhibitors with novel binding modes. This led to the discovery of the indazole series of compounds that bound in a type 1.5 binding mode to JAK and that showed good evidence of duration of action. We then followed a number of approaches to improve upon the solubility, kinase selectivity, and cellular duration of action of this series as described, leading to the preparation of **2**. The in vitro and in vivo potency, pharmacokinetic and safety profile of **2** demonstrate that it is potentially well suited for use as an inhaled or topical therapy to treat inflammatory diseases, such as COPD or psoriasis, through direct administration to the lungs or skin, while avoiding any systemic-based JAK inhibition. We believe that this profile may offer an improved safety profile for use in these disease indications over oral JAK kinase inhibitors, given the challenges associated with systemic JAK2 inhibition in particular. The pharmaceutical properties of **2** are suitable for combination with lactose in a dry powder inhaler, as well as for use in typical topical formulations. Taken together, this promising overall profile has led to the nomination of **2** as a development candidate, an inhaled therapy for COPD, and a topical therapy for psoriasis. Further information relating to the research and development of **2** will be reported in due course.

A similar approach to JAK inhibition via the inhaled route has recently been described,[30] as well as a similar approach to provide soft drug JAK inhibitors for topical use to treat psoriasis.[31]

DOI: 10.1021/acs.jmedchem.6b01634
J. Med. Chem. XXXX, XXX, XXX−XXX

EXPERIMENTAL SECTION

General Experimental. Unless otherwise indicated, all reactions were carried out under a nitrogen atmosphere, using commercially available anhydrous solvents. Thin-layer chromatography was performed on glass-backed precoated Merck silica gel (60 F254) plates, and compounds were visualized using UV light, 5% aqueous potassium permanganate, or chloroplatinic acid/potassium iodide solution. Silica gel column chromatography was carried out using 40–63 μm silica gel (Merck silica gel 60). Proton NMR spectra were measured on a Varian Inova 400 or Varian Mercury 400 spectrometer in the solvents specified. Low resolution mass spectra were recorded on either a Fisons Trio 1000, using thermospray positive ionization, or a Finnigan Navigator, using electrospray positive or negative ionization. High resolution mass spectra were recorded on a Bruker Apex II FT-MS using electrospray positive ionization. All target compounds were purified until at least >95% purity as judged by HPLC utilizing an ELSD detection system.

^{1}H nuclear magnetic resonance (NMR) spectra were in all cases consistent with the proposed structures. Characteristic chemical shifts (δ) are given in parts-per-million downfield from tetramethylsilane using conventional abbreviations for designation of major peaks: e.g., s, singlet; d, doublet; t, triplet; m, multiplet; br, broad. The mass spectra (m/z) were recorded with electrospray ionization (ESI). The following abbreviations have been used for common solvents: $CDCl_3$, deuterochloroform; DMSO-d_6, deuterodimethyl sulfoxide; methanol-d_4, deuteromethanol. Concentration of solutions after reactions and extractions involved the use of a rotary evaporator operating at a reduced pressure of ~20 Torr. LCMS analysis was carried out using the following conditions. Solvent A: 0.1% formic acid in water. Solvent B: 0.1% formic acid in acetonitrile. Column: C18 phase Phenomenex 20 mm × 4.0 mm with 3 μm particle size. Gradient: 98–10% A over 1.5 min, 0.3 min hold, 0.2 re-equilibration, 1.8 mL/min flow rate. UV: 210–450 nm DAD. Temperature: 75 °C.

PAINS Analysis. Compounds were examined for known classes of pan assay interference compounds using an in-house computational structure filter based on literature precedent.[32] None of the final compounds that were assayed for bioactivity were flagged as being potential PAINS.

Chemistry. Synthetic Procedures to 2. Additional experimental procedures for all novel compounds prepared during the course of this work can be found in the Supporting Information.

2-[6-(2-Ethyl-5-fluoro-4-hydroxyphenyl)-1*H*-indazol-3-yl]-1,4,6,7-tetrahydroimidazo[4,5-*c*]pyridin-5-yl-(5-piperidin-1-yl-pyrazin-2-yl)methanone (2). To a solution of 5-piperidin-1-ylpyrazine-2-carboxylic acid **58** (10.7 g, 51.8 mmol) in dimethylformamide (200 mL) were added *N*,*N*-diisopropylethylamine (24.6 mL, 141 mmol) and HATU (21.5 g, 56.5 mmol, and the resulting mixture was stirred at ambient temperature for 10 min before being added dropwise to a suspension of compound **55** (19.5 g, 47.1 mmol) in dimethylformamide (200 mL) over 30 min, using a further 75 mL dimethylformamide to wash the vessel. The reaction mixture was then stirred at ambient temperature for 18 h. A further portion of 5-piperidin-1-ylpyrazine-2-carboxylic acid **58** (1.07 g, 5.18 mmol) in dimethylformamide (40 mL) was treated with *N*,*N*-diisopropylethylamine (2.46 mL, 14.1 mmol) and activated with HATU (2.15 g, 5.65 mmol), and the resulting mixture was stirred at ambient temperature for 10 min before being added to the original reaction mixture which was then stirred for a further 4 h. The reaction mixture was poured onto water (1.2 L), and the pH was adjusted to 7 with sodium hydroxide solution. The resulting suspension was stirred at ambient temperature for 30 min. The precipitate was collected by filtration, washed with water (400 mL), and then dried in vacuo. The crude material was dissolved in ethanol (113 mL) and treated with a 1 M aqueous solution of sodium hydroxide. The reaction mixture was stirred at ambient temperature for 18 h. The precipitate was collected by filtration, washed with a cold solution of 1:3 1 M sodium hydroxide/ethanol (100 mL), and dried in vacuo. The residue was dissolved in water (100 mL) and treated with a 10% aqueous solution of citric acid (10 mL) to adjust the pH to 4. A few drops of 1 M sodium hydroxide solution were added to bring the pH to 7. The resulting suspension was stirred at ambient temperature for 1 h and the solid collected by filtration, washed with water, and then dried in vacuo to give the title compound **2** (13.86 g, 89%). ^{1}H NMR (400 MHz, DMSO-d_6) δ 9.90 (br s, 1H), 8.44 (s, 1H), 8.31 (d, J = 1.17 Hz, 1H), 8.27 (br s, 1H), 7.58 (s, 1H), 7.32 (d, J = 7.42 Hz, 1H), 7.05 (d, J = 11.72 Hz, 1H), 6.94 (d, J = 9.18 Hz, 1H), 4.96 (br s, 1H), 4.82 (br s, 1H), 4.02 (t, J = 5.37 Hz, 2H), 3.66–3.75 (m, 4H), 2.92 (br s, 2H), 2.42–2.49 (m, 2H), 1.66 (d, J = 4.69 Hz, 2H), 1.58 (d, J = 3.90 Hz, 4H), 1.02 (t, J = 7.52 Hz, 3H). LCMS found 567 $[M + H]^+$. HRMS calcd for $C_{31}H_{32}FN_8O_2$: 567.2627. Found $[M + H]^+$: 567.2621.

6-Bromo-1-(tetrahydropyran-2-yl)-1*H*-indazole-3-carbonitrile (47). To a solution of 6-bromo-1*H*-indazole-3-carbaldehyde **25** (13.97 g, 61.9 mmol) in dichloromethane (150 mL) was added *p*-toluenesulfonic acid (2.36 g, 12.4 mmol), and the mixture was cooled to 0 °C. 3,4-Dihydro-2*H*-pyran (8.47 mL, 92.8 mmol) was added dropwise to the solution, and the reaction was stirred at ambient temperature overnight. The reaction mixture was diluted with dichloromethane (200 mL) and washed with a solution of saturated aqueous sodium hydrogen carbonate (500 mL). The aqueous layer was re-extracted with dichloromethane (500 mL), and the combined organic layers were washed with brine (2 × 1 L), dried over anhydrous magnesium sulfate, and concentrated in vacuo. The crude material was refluxed in cyclohexane (20 mL) and filtered while hot. The filtrate was concentrated in vacuo, and the residue was stirred in heptane for 48 h. The resulting solid was collected by filtration to give 6-bromo-1-(tetrahydropyran-2-yl)-1*H*-indazole-3-carbaldehyde (13.87 g, 73%). ^{1}H NMR (400 MHz, $CDCl_3$) δ 10.19–10.25 (m, 1H), 8.16 (d, J = 8.59 Hz, 1H), 7.88 (d, J = 0.98 Hz, 1H), 7.46 (dd, J = 1.56, 8.59 Hz, 1H), 5.78 (dd, J = 2.83, 8.69 Hz, 1H), 4.95 (dd, J = 2.64, 4.78 Hz, 2H), 3.96–4.04 (m, 2H), 3.88 (ddd, J = 3.42, 7.32, 11.13 Hz, 3H), 3.74–3.82 (m, 1H), 3.46–3.57 (m, 3H), 2.48–2.61 (m, 2H), 2.08–2.28 (m, 3H), 1.81–1.95 (m, 4H), 1.71–1.80 (m, 6H), 1.48–1.66 (m, 16H). LCMS found 309 $[M + H]^+$. To a solution of 6-bromo-1-(tetrahydropyran-2-yl)-1*H*-indazole-3-carbaldehyde (60 g, 194 mmol) in acetonitrile (1.5 L) were added triethylamine (68.5 mL, 485 mmol) and hydroxylamine hydrochloride (20 g, 291 mmol). The reaction was heated at 60 °C for 3 h. The reaction was cooled to 0 °C, further triethylamine (220 mL, 1.55 mol) was added, and TFAA (109 mL, 776 mmol) was added dropwise. The reaction was allowed to warm to ambient temperature and stirred for 2 h. Water (2 L) was added to the reaction mixture, and the resulting solid was collected by filtration. The solid was dissolved in dichloromethane (1 L), and the resulting solution was washed with water (2 × 500 mL). The organic layer was dried over anhydrous magnesium sulfate and concentrated in vacuo to give the title compound **47** (58.59 g, 99%). ^{1}H NMR (400 MHz, $CDCl_3$) δ 7.93 (d, J = 0.98 Hz, 1H), 7.69 (d, J = 8.79 Hz, 1H), 7.46 (dd, J = 1.56, 8.79 Hz, 1H), 5.76 (dd, J = 2.93, 8.20 Hz, 1H), 3.88–3.96 (m, 1H), 3.71–3.81 (m, 1H), 2.40–2.54 (m, 1H), 2.05–2.23 (m, 2H), 1.68–1.85 (m, 3H). LCMS found 306 $[M + H]^+$.

6-[2-Ethyl-5-fluoro-4-(2-trimethylsilanylethoxymethoxy)-phenyl]-1-(tetrahydropyran-2-yl)-1*H*-indazole-3-carboximidic Acid Methyl Ester (48). To a solution of **47** (28.5 g, 93 mmol) and **51** (73.8 g, 112 mmol) in 1,4-dioxane (500 mL) was added a solution of potassium phosphate (59.2 g, 279 mmol) in water (120 mL). The mixture was degassed with nitrogen, and then tetrakis(triphenylphosphine)palladium (0) (10.8 g, 9.3 mmol) was added. The reaction mixture was heated at 110 °C for 18 h. The reaction mixture was concentrated in vacuo, and the residue was redissolved in ethyl acetate (1 L) and filtered through Arbocel, washing with ethyl acetate (2 × 500 mL). The combined organic phases were concentrated in vacuo. The residue was purified by column chromatography on silica gel, eluting with 10% ethyl acetate in heptane to give 6-[2-ethyl-5-fluoro-4-(2-trimethylsilanylethoxymethoxy)phenyl]-1-(tetrahydropyran-2-yl)-1*H*-indazole-3-carbonitrile (37.4 g, 81%). ^{1}H NMR (400 MHz, $CDCl_3$) δ 7.85 (dd, J = 0.78, 8.40 Hz, 1H), 7.62 (d, J = 0.98 Hz, 1H), 7.30 (dd, J = 1.27, 8.30 Hz, 1H), 7.18 (d, J = 8.40 Hz, 1H), 7.15–7.23 (m, 1H), 7.00 (d, J = 11.52 Hz, 1H), 5.82 (dd, J = 2.73, 8.59 Hz, 1H), 5.30–5.35 (m, 2H), 3.94–4.01 (m, 1H), 3.83–3.91 (m, 2H), 3.75 (ddd, J = 3.71, 8.64, 11.86 Hz, 1H), 2.53 (q, J = 7.35 Hz, 2H), 2.12–2.25 (m, 2H), 1.66–1.89 (m, 3H), 1.11 (t, J = 7.52 Hz, 3H), 1.02 (dd,

DOI: 10.1021/acs.jmedchem.6b01634
J. Med. Chem. XXXX, XXX, XXX–XXX

J = 7.71, 8.88 Hz, 2H), 0.01−0.09 (m, 9H). To a solution of 6-[2-ethyl-5-fluoro-4-(2-trimethylsilanylethoxymethoxy)phenyl]-1-(tetrahydropyran-2-yl)-1*H*-indazole-3-carbonitrile (37.42 g, 75.6 mmol) in methanol (700 mL) was added sodium methoxide (12.21 g, 226.8 mmol), and the reaction mixture was then stirred at ambient temperature for 18 h. The solvent was removed in vacuo, and the residue was partitioned between ethyl acetate (1 L) and water (500 mL). The organic layer was washed with water (500 mL), dried over anhydrous magnesium sulfate, and concentrated in vacuo to give the title compound **48** (37.26g, 94%). ^{1}H NMR (400 MHz, $CDCl_3$) δ 8.41−8.61 (m, 1H), 8.05−8.12 (m, 1H), 7.50 (s, 1H), 7.14−7.23 (m, 2H), 7.03 (d, J = 11.52 Hz, 1H), 5.76 (dd, J = 2.73, 9.18 Hz, 1H), 4.06−4.12 (m, 3H), 4.00−4.06 (m, 1H), 3.82−3.91 (m, 2H), 3.70−3.79 (m, 1H), 3.50 (s, 2H), 2.49−2.66 (m, 2H), 2.06−2.25 (m, 2H), 1.63−1.88 (m, 4H), 1.10 (t, J = 7.52 Hz, 3H), 0.97−1.06 (m, 2H), −0.02 to 0.13 (m, 9H). LCMS found 528 $[M + H]^+$.

2-[2-Ethyl-5-fluoro-4-(2-trimethylsilanylethoxymethoxy)-phenyl]-4,4,5,5-tetramethyl[1,3,2]dioxaborolane (51). To a solution of 5-ethyl-2-fluorophenol **50** (76.36g, 545 mmol) in acetonitrile (2.5 L) was added copper(II) bromide (361.5 g, 1.62 mol). The resulting suspension was stirred at ambient temperature overnight. The solvent was removed in vacuo, and the residue was suspended in ethyl acetate (3 L) and filtered through a pad of Arbocel. The filtrate was washed with water (2 L) and brine (2 L), dried over anhydrous magnesium sulfate, and concentrated in vacuo to give 4-bromo-5-ethyl-2-fluorophenol (119 g, 100%). ^{1}H NMR (400 MHz, $CDCl_3$) δ 7.29 (d, J = 2.34 Hz, 1H), 6.92 (d, J = 9.37 Hz, 1H), 5.21 (br s, 1H), 2.69 (q, J = 7.41 Hz, 2H), 1.22 (t, J = 7.61 Hz, 3H). To a solution of 4-bromo-5-ethyl-2-fluorophenol (80 g, 365 mmol) in DCM (1 L) was added *N*,*N*-diisopropylethylamine (70 mL, 401 mmol) and (2-trimethylsilyl)ethoxymethyl chloride (71 mL, 401 mmol). The resulting solution was stirred at ambient temperature for 18 h. The reaction mixture was washed with water (1 L), dried over anhydrous magnesium sulfate, and concentrated in vacuo to yield the crude product. This material was purified by silica gel chromatography, eluting with 30% DCM in heptane to give [2-(4-bromo-5-ethyl-2-fluorophenoxymethoxy)ethyl]trimethylsilane. (109.8 g, 86%). ^{1}H NMR (400 MHz, $CDCl_3$) δ 7.25−7.30 (m, 1H), 7.07−7.12 (m, 1H), 5.24 (s, 2H), 3.77−3.85 (m, 2H), 2.69 (q, J = 7.48 Hz, 2H), 1.21 (t, J = 7.52 Hz, 3H), 0.94−1.01 (m, 2H), 0.01−0.05 (m, 9H). To a solution of [2-(4-bromo-5-ethyl-2-fluorophenoxymethoxy)ethyl]-trimethylsilane (105g, 300.6 mmol) in dioxane (1 L) were added bis(pinacolato)diboron (76.4 g, 300.6 mmol) and potassium acetate (88.5 g, 902 mmol). The resulting suspension was degassed with nitrogen, Pd(dppf)Cl_2 (24.54 g, 30.1 mmol) was added, and the reaction was heated at reflux for 18 h. The reaction was cooled to ambient temperature, and the solvent was removed in vacuo. The resulting black solid was suspended in ethyl acetate (2 L) and filtered through Arbocel, washing with further ethyl acetate. The filtrate was washed with water (1.5 L) and brine (1.5 L), dried over anhydrous magnesium sulfate, and concentrated in vacuo to give the title compound **51** (155.5 g, 130%) that was used crude in the next step. ^{1}H NMR (400 MHz, $CDCl_3$) δ 7.47 (d, J = 12.10 Hz, 1H), 6.98−7.04 (m, 1H), 5.27 (s, 2H), 3.77−3.82 (m, 2H), 2.85 (q, J = 7.54 Hz, 2H), 1.32 (s, 12H), 1.16 (t, J = 7.61 Hz, 3H), 0.91−0.99 (m, 2H), −0.02 to 0.02 (m, 9H).

4,4-Diethoxy-3-[6-[2-ethyl-5-fluoro-4-(2-trimethylsilanyl-ethoxymethoxy)phenyl]-1-(tetrahydropyran-2-yl)-1*H*-indazole-3-carboximidoyl]aminopiperidine-1-carboxylic Acid *tert*-Butyl Ester (54). To a solution of **48** (31.4 g, 59.5 mmol) in ethanol (140 mL) was added a solution of **57** (US-2004/0229862, 18.02 g, 62.48 mmol) in ethanol (100 mL). Acetic acid (6.81 mL, 119 mmol) was added, and the reaction mixture was heated at 50 °C for 18 h. The reaction mixture was concentrated in vacuo and azeotroped with toluene (100 mL) to give the title compound **54** (54.7 g, 117%) which was used as is without further purification. ^{1}H NMR (400 MHz, $CDCl_3$) δ 8.23 (br s, 1H), 7.51 (br s, 1H), 7.32−7.43 (m, 2H), 7.18−7.30 (m, 4H), 7.16 (d, J = 8.40 Hz, 1H), 7.04 (d, J = 11.52 Hz, 1H), 5.77 (br s, 1H), 5.31 (d, J = 8.20 Hz, 2H), 4.04 (t, J = 10.45 Hz, 1H), 3.82−3.92 (m, 2H), 3.48−3.82 (m, 7H), 2.81 (br s, 1H), 2.67 (br s, 3H), 2.55 (q, J = 7.42 Hz, 2H), 2.09−2.32 (m, 3H), 1.92 (br s, 2H), 1.65−1.84 (m, 3H), 1.14−1.24 (m, 5H), 1.10 (t, J = 7.52 Hz, 3H), 0.98−1.04 (m, 2H), 0.00−0.07 (m, 9H). LCMS found 784 $[M + H]^+$.

5-Ethyl-2-fluoro-4-[3-(4,5,6,7-tetrahydro-1*H*-imidazo[4,5-*c*]-pyridin-2-yl)-1*H*-indazol-6-yl]phenol Dihydrochloric Acid Salt (55). To a solution of **54** (46.65 g, 55.27 mmol) in ethanol (200 mL) was added concentrated hydrochloric acid (12M, 100 mL, 1.2 mol), and the resulting solution was stirred at ambient temperature for 18 h. The reaction mixture was concentrated in vacuo and azeotroped with toluene (100 mL) and dichloromethane (2 × 100 mL). The resulting gum was dried under vacuum for 3 h. The crude material was triturated in acetonitrile (300 mL), and the resulting solid was collected by filtration. The solid was dissolved in ethanol (250 mL) and treated with concentrated hydrochloric acid (12 M, 77.2 mL, 927 mmol). The resulting solution was heated at 40 °C for 18 h, then at 50 °C for 2 h. The solvents were removed in vacuo, and the resulting gum was triturated in acetonitrile (200 mL). The solid that formed was collected by filtration, washed with further acetonitrile (200 mL), and dried under vacuum to give the title compound **55** (23.5 g, 88% dihydrochloride salt). ^{1}H NMR (400 MHz, CD_3OD) δ 8.22 (d, J = 8.40 Hz, 1H), 7.59 (s, 1H), 7.33−7.41 (m, 1H), 6.95 (d, J = 11.52 Hz, 1H), 6.91 (d, J = 8.98 Hz, 1H), 4.56 (s, 2H), 3.73 (t, J = 6.05 Hz, 2H), 3.23 (t, J = 5.86 Hz, 2H), 2.53 (q, J = 7.61 Hz, 2H), 1.02−1.10 (m, 3H). LCMS found 378 $[M + H]^+$.

■ ASSOCIATED CONTENT

Supporting Information

The Supporting Information is available free of charge on the ACS Publications website at DOI: 10.1021/acs.jmedchem.6b01634.

Molecular formula strings and some data (CSV)

General chemistry experimental procedures; all synthetic procedures and analytical data with synthesis schemes; selected HPLC and NMR spectra of **2**; kinase inhibition panels for selected compounds and polypharmacology and broad kinase inhibition profile for **2**; biology experimental procedures; table of crystallography information (PDF)

Accession Codes

PDB codes are the following: 3LXK for **1**, 5TQ7 for **4**, 5TQ3 for **5**, 5TQ4 for **13**, 5TQ5 for **16**, 5TQ8 for **2**. Authors will release the atomic coordinates and experimental data upon article publication.

■ AUTHOR INFORMATION

Corresponding Authors

*P.J.: e-mail, peter.jones2@pfizer.com.

*R.I.S.: e-mail, ian.storer@astrazeneca.com.

ORCID

Peter Jones: 0000-0001-8637-9530

Present Addresses

◆R.I.S.: AstraZeneca, 310 Cambridge Science Park, Milton Road, Cambridge, CB4 0FZ, U.K.

¶Y.A.S.: UCB Pharma, Allee de la Recherche 60, 1070 Anderlecht, Brussels, Belgium.

∞F.M.W.: B. Braun Melsungen AG, Pfieffewiesen, 34212 Melsungen, Germany.

×G.A.W.: Sandexis Medicinal Chemistry Ltd., Innovation House, Discovery Park, Sandwich, Kent CT13 9FF, U.K.

◇K.S.E.: Target Discovery Institute, Nuffield Department of Medicine, University of Oxford, Roosevelt Drive, Oxford, OX3 7FZ, U.K.

DOI: 10.1021/acs.jmedchem.6b01634
J. Med. Chem. XXXX, XXX, XXX−XXX

△T.M.: Department of Chemistry and Skaggs Institute for Chemical Biology, The Scripps Research Institute, 10550 North Torrey Pines Road, La Jolla, California 92037, U.S.
▲C.M.D.: Xenon Pharmaceuticals, 3650 Gilmore Way, Burnaby, BC, V5G 4W8, Canada.
∀D.G.B.: School of Biosciences, University of Kent, Canterbury, Kent, CT2 7NJ, U.K.

Author Contributions

The manuscript was written through contributions of all authors. All authors have given approval to the final version of the manuscript.

Notes

The authors declare the following competing financial interest(s): The authors were all full-time employees of Pfizer at the time this work was completed, and all funding for the work was provided by Pfizer.

■ ACKNOWLEDGMENTS

This research used resources at the Industrial Macromolecular Crystallography Association Collaborative Access Team (IMCA-CAT) beamline 17-ID, supported by the companies of the Industrial Macromolecular Crystallography Association through a contract with Hauptman-Woodward Medical Research Institute. This research used resources of the Advanced Photon Source, a U.S. Department of Energy (DOE) Office of Science User Facility operated for the DOE Office of Science by Argonne National Laboratory under Contract DE-AC02-06CH11357. Use of the LS-CAT Sector 21 was supported by the Michigan Economic Development Corporation and the Michigan Technology Tri-Corridor (Grant 085P1000817). The Advanced Light Source is supported by the Director, Office of Science, Office of Basic Energy Sciences, of the U.S. Department of Energy under Contract DE-AC02-05CH11231. We thank Diamond Light Source for access to beamline I04-1 that contributed to the results presented here. We thank Adrian Barnard and Hinnah Campwala for in vitro assays. We thank Katy Hulland, David Lamb, Susan Fish, Cedric Hubeau, and John Kubera for in vivo studies.

■ ABBREVIATIONS USED

AcOH, acetic acid; br, broad; $CDCl_3$, chloroform-d_1; CI, confidence interval (95% unless otherwise stated); δ, chemical shift; d, doublet; DMSO, dimethylsulfoxide; DoA, duration of action; ELSD, evaporative light scattering detector; ESI, electrospray ionization; EtOAc, ethyl acetate; Et_2O, diethyl ether; GM-CSF, granulocyte macrophage colony-stimulating factor; h, hour(s); HPLC, high performance liquid chromatography; HRMS, high resolution mass spectrum; IFN, interferon; IL, interleukin; i.t., intratracheal; JAK, Janus kinase; Tyk, tyrosine linase; LRMS, low resolution mass spectrum; M, molarity; m, multiplet; Me, methyl; MeOH, methanol; mg, milligram; min, minute(s); MHz, megahertz; mL, milliliter; mmol, millimole; m/z, mass-to-charge ratio; N, normal concentration; NMR, nuclear magnetic resonance; t_R, retention time; s, singlet; t, triplet; UV-TIC, ultraviolet total ion count

■ REFERENCES

(1) O'Shea, J. J.; Kontzias, A.; Yamaoka, K.; Tanaka, Y.; Laurence, A. Janus kinase inhibitors in autoimmune diseases. *Ann. Rheum. Dis.* **2013**, *72* (Suppl. 2), ii111−ii115.

(2) Clark, J. D.; Flanagan, M. E.; Telliez, J.-B. Discovery and development of janus kinase (JAK) inhibitors for inflammatory diseases. *J. Med. Chem.* **2014**, *57* (12), 5023−5038.

(3) (a) Flanagan, M. E.; Blumenkopf, T. A.; Brissette, W. H.; Brown, M. F.; Casavant, J. M.; Chang, S.-P.; Doty, J. L.; Elliott, E. A.; Fisher, M. B.; Hines, M.; Kent, C.; Kudlacz, E. M.; Lillie, B. M.; Magnuson, K. S.; McCurdy, S. P.; Munchhof, M. J.; Perry, B. D.; Sawyer, P. S.; Strelevitz, T. J.; Subramanyam, C.; Sun, J.; Whipple, D. A.; Changelian, P. S. Discovery of CP-690,550: a potent and selective janus kinase (JAK) inhibitor for the treatment of autoimmune diseases and organ transplant rejection. *J. Med. Chem.* **2010**, *53* (24), 8468−8484. (b) News in brief. *Nat. Rev. Drug Discovery* **2012**, *11* (12), 895, DOI: 10.1038/nrd3911 (c) Compound **1** (catalog no. PZ0017) is available from Sigma Aldrich..

(4) (a) Burmester, G. R.; Blanco, R.; Charles-Schoeman, C.; Wollenhaupt, J.; Zerbini, C.; Benda, B.; Gruben, D.; Wallenstein, G.; Krishnaswami, S.; Zwillich, S. H.; Koncz, T.; Soma, K.; Bradley, J.; Mebus, C. Tofacitinib (CP-690,550) in combination with methotrexate in patients with active rheumatoid arthritis with an inadequate response to tumour necrosis factor inhibitors: a randomised phase 3 trial. *Lancet* **2013**, *381* (9865), 451−460. (b) Fleischmann, R.; Kremer, J.; Cush, J.; Schulze-Koops, H.; Connell, C. A.; Bradley, J. D.; Gruben, D.; Wallenstein, G. V.; Zwillich, S. H.; Kanik, K. S. Placebo-controlled trial of tofacitinib monotherapy in rheumatoid arthritis. *N. Engl. J. Med.* **2012**, *367* (6), 495−507. (c) Kremer, J.; Li, Z.-G.; Hall, S.; Fleischmann, R.; Genovese, M.; Martin-Mola, E.; Isaacs, J. D.; Gruben, D.; Wallenstein, G.; Krishnaswami, S.; Zwillich, S. H.; Koncz, T.; Riese, R.; Bradley, J. Tofacitinib in combination with nonbiologic disease-modifying antirheumatic drugs in patients with active rheumatoid arthritis: a randomized trial. *Ann. Intern. Med.* **2013**, *159* (4), 253−261. (d) Lee, E. B.; Fleischmann, R.; Hall, S.; Wilkinson, B.; Bradley, J. D.; Gruben, D.; Koncz, T.; Krishnaswami, S.; Wallenstein, G. V.; Zang, C.; Zwillich, S. H.; van Vollenhoven, R. F. Tofacitinib versus methotrexate in rheumatoid arthritis. *N. Engl. J. Med.* **2014**, *370* (25), 2377−2386. (e) van der Heijde, D.; Tanaka, Y.; Fleischmann, R.; Keystone, E.; Kremer, J.; Zerbini, C.; Cardiel, M. H.; Cohen, S.; Nash, P.; Song, Y.-W.; Tegzova, D.; Wyman, B. T.; Gruben, D.; Benda, B.; Wallenstein, G.; Krishnaswami, S.; Zwillich, S. H.; Bradley, J. D.; Connell, C. A. Tofacitinib (CP-690,550) in patients with rheumatoid arthritis receiving methotrexate: twelve-month data from a twenty-four-month phase III randomized radiographic study. *Arthritis Rheum.* **2013**, *65* (3), 559−570. (f) van Vollenhoven, R. F.; Fleischmann, R.; Cohen, S.; Lee, E. B.; Meijide, J. A. G.; Wagner, S.; Forejtova, S.; Zwillich, S. H.; Gruben, D.; Koncz, T.; Wallenstein, G. V.; Krishnaswami, S.; Bradley, J. D.; Wilkinson, B. Tofacitinib or adalimumab versus placebo in rheumatoid arthritis. *N. Engl. J. Med.* **2012**, *367* (6), 508−519.

(5) (a) Bachelez, H.; van de Kerkhof, P. C. M.; Strohal, R.; Kubanov, A.; Valenzuela, F.; Lee, J.-H.; Yakusevich, V.; Chimenti, S.; Papacharalambous, J.; Proulx, J.; Gupta, P.; Tan, H.; Tawadrous, M.; Valdez, H.; Wolk, R. Tofacitinib versus etanercept or placebo in moderate-to-severe chronic plaque psoriasis: a phase 3 randomised non-inferiority trial. *Lancet* **2015**, *386* (9993), 552−561. (b) Bissonnette, R.; Iversen, L.; Sofen, H.; Griffiths, C. E. M.; Foley, P.; Romiti, R.; Bachinsky, M.; Rottinghaus, S. T.; Tan, H.; Proulx, J.; Valdez, H.; Gupta, P.; Mallbris, L.; Wolk, R. Tofacitinib withdrawal and retreatment in moderate-to-severe chronic plaque psoriasis: a randomized controlled trial. *Br. J. Dermatol.* **2015**, *172* (5), 1395−1406. (c) Papp, K. A.; Krueger, J. G.; Feldman, S. R.; Langley, R. G.; Thaci, D.; Torii, H.; Tyring, S.; Wolk, R.; Gardner, A.; Mebus, C.; Tan, H.; Luo, Y.; Gupta, P.; Mallbris, L.; Tatulych, S. Tofacitinib, an oral Janus kinase inhibitor, for the treatment of chronic plaque psoriasis: Long-term efficacy and safety results from 2 randomized phase-III studies and 1 open-label long-term extension study. *J. Am. Acad. Dermatol.* **2016**, *74* (5), 841−850. (d) Papp, K. A.; Menter, M. A.; Abe, M.; Elewski, B.; Feldman, S. R.; Gottlieb, A. B.; Langley, R.; Luger, T.; Thaci, D.; Buonanno, M.; Gupta, P.; Proulx, J.; Lan, S.; Wolk, R. Tofacitinib, an oral Janus kinase inhibitor, for the treatment

DOI: 10.1021/acs.jmedchem.6b01634
J. Med. Chem. XXXX, XXX, XXX−XXX

of chronic plaque psoriasis: results from two randomized, placebo-controlled, phase III trials. *Br. J. Dermatol.* **2015**, *173* (4), 949−961.
(6) (a) Sandborn, W. J.; Ghosh, S.; Panes, J.; Vranic, I.; Su, C.; Rousell, S.; Niezychowski, W. Tofacitinib, an oral Janus kinase inhibitor, in active ulcerative colitis. *N. Engl. J. Med.* **2012**, *367* (7), 616−624. (b) Sandborn, W. J.; D'Haens, G.; Vermeir, S.; Schreiber, S.; Danese, S.; Panes, J.; Faegan, B. G.; Reinisch, W.; Niezychowski, W.; Friedman, G.; Lawendy, N.; Yu, D.; Woodworth, D.; Mukherjee, A.; Healey, P.; Zhang, H.; Su, C. Efficacy and safety of oral tofacitinib as induction therapy in patients with moderate-to-severe ulcerative colitis: results from 2 phase 3 randomised controlled trials. *J. Crohn's Colitis* **2016**, *10* (OP019), S15.
(7) (a) D'Haens, G.; Higgins, P.; Colombel, J.; Feagan, B.; Moscariello, M.; Chan, G.; Healey, P.; Niezychowski, W.; Wang, W.; Marren, A.; Maller, E. Efficacy and safety of oral tofacitinib for maintenance therapy in patients with moderate-to-severe Crohn's disease: results of a Phase 2b randomised placebo-controlled trial. *J. Crohns Colitis* **2016**, *10* (OP021), S17. (b) Panes, J.; Su, C.; Bushmakin, A. G.; Cappelleri, J. C.; Mamolo, C.; Healey, P. Randomized trial of tofacitinib in active ulcerative colitis: analysis of efficacy based on patient-reported outcomes. *BMC Gastroenterol.* **2015**, *15*, 14. (c) Sandborn, W. J.; Ghosh, S.; Panes, J.; Vranic, I.; Wang, W.; Niezychowski, W. A Phase 2 study of tofacitinib, an oral janus kinase inhibitor, in patients with Crohn's disease. *Clin. Gastroenterol. Hepatol.* **2014**, *12* (9), 1485−1493.
(8) Pfizer press release: Pfizer announces positive top-line results from second phase 3 trial of oral Xeljanz (tofacitinib citrate) in adults with psoriatic arthritis. June 7, 2016; www.pfizer.com.
(9) van der Heijde, D. D. A.; Wei, J. C.; Drescher, E.; Fleishaker, D.; Hendrikx, T.; Li, D.; Menon, S.; Kanik, K. Tofacitinib in patients with ankylosing spondylitis: a phase 2, 16-week, randomized, placebo-controlled, dose-ranging study. *Arthritis Rheumatol.* **2015**, *67*, 5L.
(10) Wollenhaupt, J.; Silverfield, J.; Lee, E. B.; Curtis, J. R.; Wood, S. P.; Soma, K.; Nduaka, C. I.; Benda, B.; Gruben, D.; Nakamura, H.; Komuro, Y.; Zwillich, S. H.; Wang, L.; Riese, R. J. Safety and efficacy of tofacitinib, an oral janus kinase inhibitor, for the treatment of rheumatoid arthritis in open-label, longterm extension studies. *J. Rheumatol.* **2014**, *41* (5), 837−852.
(11) (a) Coe, J. W.; Dehnhardt, C. M.; Jones, P.; Kortum, S. W.; Sabnis, Y. A.; Wakenhut, F. M.; Whitlock, G. A. Indazoles. WO2013014567 A1, 2013. (b) Compound **2** (catalog no. PZ0324) is available from Sigma Aldrich..
(12) Barnes, P. J. New anti-inflammatory targets for chronic obstructive pulmonary disease. *Nat. Rev. Drug Discovery* **2013**, *12* (7), 543−59.
(13) (a) Jones, L. H.; Baldock, H.; Bunnage, M. E.; Burrows, J.; Clarke, N.; Coghlan, M.; Entwistle, D.; Fairman, D.; Feeder, N.; Fulton, C.; Hilton, L.; James, K.; Jones, R. M.; Kenyon, A. S.; Marshall, S.; Newman, S. D.; Osborne, R.; Patel, S.; Selby, M. D.; Stuart, E. F.; Trevethick, M. A.; Wright, K. N.; Price, D. A. Inhalation by design: dual pharmacology β-2 agonists/M3 antagonists for the treatment of COPD. *Bioorg. Med. Chem. Lett.* **2011**, *21* (9), 2759−2763. (b) Hilton, L.; Osborne, R.; Kenyon, A. S.; Baldock, H.; Bunnage, M. E.; Burrows, J.; Clarke, N.; Coghlan, M.; Entwistle, D.; Fairman, D.; Feeder, N.; James, K.; Jones, R. M.; Laouar, N.; Lunn, G.; Marshall, S.; Newman, S. D.; Patel, S.; Selby, M. D.; Spence, F.; Stuart, E. F.; Summerhill, S.; Trevethick, M. A.; Wright, K. N.; Yeadon, M.; Price, D. A.; Jones, L. H. Optimized glucuronidation of dual pharmacology β-2 agonists/M3 antagonists for the treatment of COPD. *MedChemComm* **2011**, *2*, 870−876. (c) Glossop, P. A.; Lane, C. A. L.; Price, D. A.; Bunnage, M. E.; Lewthwaite, R. A.; James, K.; Brown, A. D.; Yeadon, M.; Perros-Huguet, C.; Trevethick, M. A.; Clarke, N. P.; Webster, R.; Jones, R. M.; Burrows, J. L.; Feeder, N.; Taylor, S. C. J.; Spence, F. J. Inhalation by design: novel ultra-long-acting β2-adrenoreceptor agonists for inhaled once-daily treatment of asthma and chronic obstructive pulmonary disease that utilize a sulfonamide agonist headgroup. *J. Med. Chem.* **2010**, *53* (18), 6640−6652. (d) Millan, D. S.; Bunnage, M. E.; Burrows, J. L.; Butcher, K. J.; Dodd, P. G.; Evans, T. J.; Fairman, D. A.; Hughes, S. J.; Kilty, I. C.; Lemaitre, A.; Lewthwaite, R. A.; Mahnke, A.; Mathias, J. P.; Philip, J.; Smith, R. T.; Stefaniak, M. H.; Yeadon, M.; Phillips, C. Design and synthesis of inhaled p38 inhibitors for the treatment of chronic obstructive pulmonary disease. *J. Med. Chem.* **2011**, *54* (22), 7797−7814.
(14) Compound **3** (catalog no. PZ0151) is available from Sigma Aldrich.
(15) Pan, Y.; Karns, K.; Herr, A. E. Microfluidic electrophoretic mobility shift assays for quantitative biochemical analysis. *Electrophoresis* **2014**, *35* (15), 2078−2090.
(16) Zhao, Z.; Wu, H.; Wang, L.; Liu, Y.; Knapp, S.; Liu, Q.; Gray, N. S. Exploration of type II binding mode: a privileged approach for kinase inhibitor focused drug discovery? *ACS Chem. Biol.* **2014**, *9* (6), 1230−1241.
(17) (a) Berman, H. M.; Henrick, K.; Nakamura, H. Announcing the worldwide Protein Data Bank. *Nat. Struct. Biol.* **2003**, *10*, 980. (b) Rose, P. W.; Prlic, A.; Bi, C.; Bluhm, W. F.; Christie, C. H.; Dutta, S.; Green, R. K.; Goodsell, D. S.; Westbrook, J. D.; Woo, J.; Young, J.; Zardecki, C.; Berman, H. M.; Bourne, P. E.; Burley, S. K. The RCSB Protein Data Bank: views of structural biology for basic and applied research and education. *Nucleic Acids Res.* **2015**, *43*, D345−D356.
(18) Kania, R. S.; Bender, S. L.; Borchardt, A. J.; Braganza, J. F.; Cripps, S. J.; Hua, Y.; Johnson, M. D.; Johnson, T. O., Jr.; Luu, H. T.; Palmer, C. L.; Reich, S. H.; Tempczyk-russell, A. M.; Teng, M.; Thomas, C.; Varney, M. D.; Wallace, M. B. Indazole compounds and pharmaceutical compositions for inhibiting protein kinases, and methods for their use. WO2001002369, 2001.
(19) Zuccotto, F.; Ardini, E.; Casale, E.; Angiolini, M. Through the "gatekeeper door": exploiting the active kinase conformation. *J. Med. Chem.* **2010**, *53* (7), 2681−2694.
(20) Thorarensen, A.; Banker, M. E.; Fensome, A.; Telliez, J.-B.; Juba, B.; Vincent, F.; Czerwinski, R. M.; Casimiro-Garcia, A. ATP-mediated kinome selectivity: the missing link in understanding the contribution of individual JAK kinase isoforms to cellular signaling. *ACS Chem. Biol.* **2014**, *9* (7), 1552−1558.
(21) Ritchie, T. J.; MacDonald, S. J. F.; Young, R. J.; Pickett, S. D. The impact of aromatic ring count on compound developability: further insights by examining carbo- and hetero-aromatic and -aliphatic ring types. *Drug Discovery Today* **2011**, *16* (3/4), 164−171.
(22) Walker, M. A. Novel tactics for designing water-soluble molecules in drug discovery. *Expert Opin. Drug Discovery* **2014**, *9* (12), 1421−1433.
(23) Lovering, F.; Bikker, J.; Humblet, C. Escape from flatland: increasing saturation as an approach to improving clinical success. *J. Med. Chem.* **2009**, *52* (21), 6752−6756.
(24) Patton, J. S.; Byron, P. R. Inhaling medicines: delivering drugs to the body through the lungs. *Nat. Rev. Drug Discovery* **2007**, *6* (1), 67−74.
(25) Hsu, L.; Armstrong, A. W. JAK inhibitors: treatment efficacy and safety profile in patients with psoriasis. *J. Immunol. Res.* **2014**, *2014*, 1−7.
(26) Patricelli, M. P.; Szardenings, A. K.; Liyanage, M.; Nomanbhoy, T. K.; Wu, M.; Weissig, H.; Aban, A.; Chun, D.; Tanner, S.; Kozarich, J. W. Functional interrogation of the kinome using nucleotide acyl phosphates. *Biochemistry* **2007**, *46* (2), 350−358.
(27) Siewert, E.; Muller-Esterl, W.; Starr, R.; Heinrich, P. C.; Schaper, F. Different protein turnover of interleukin-6-type cytokine signalling components. *Eur. J. Biochem.* **1999**, *265* (1), 251−257.
(28) Diez, A.; Voldoire, A.; Lopez, I.; Rubiralta, M.; Segarra, V.; Pages, L.; Palacios, J. M. Synthetic applications of 2-aryl-4-piperidones. X. Synthesis of 3-aminopiperidines, potential substances P antagonists. *Tetrahedron* **1995**, *51* (17), 5143−56.
(29) Flohr, A.; Jakob-Roetne, R.; Norcross, R. D.; Riemer, C. Imidazolyl benzothiazoles as adenosine receptor ligands, processes for their preparations, pharmaceutical formulations and uses thereof. US20040229862, 2004.
(30) Ramis, I.; Calama, E.; Domenech, A.; Carreno, C.; Calaf, E.; Cordoba, M.; Alberti, J.; De Alba, J.; Bach, J.; Prats, N.; Miralpeix, M. New inhaled JAK inhibitor LAS194046 inhibits allergen-induced

DOI: 10.1021/acs.jmedchem.6b01634
J. Med. Chem. XXXX, XXX, XXX−XXX

airway inflammation in Brown Norway rats. *Eur. Respir. J.* **2014**, *44* (Suppl. 58), 1508.
(31) Ritzen, A.; Soerensen, M. D.; Dack, K. N.; Greve, D. R.; Jerre, A.; Carnerup, M. A.; Rytved, K. A.; Bagger-Bahnsen, J. Fragment-based discovery of 6-arylindazole JAK inhibitors. *ACS Med. Chem. Lett.* **2016**, *7* (6), 641−646.
(32) Baell, J. B.; Holloway, G. A. New substructure filters for removal of pan assay interference compounds (PAINS) from screening libraries and for their exclusion in bioassays. *J. Med. Chem.* **2010**, *53* (7), 2719−2740.

DOI: 10.1021/acs.jmedchem.6b01634
J. Med. Chem. XXXX, XXX, XXX−XXX